



**HAL**  
open science

## Characterization and modeling of laser transmission welded polyetherketoneketone (PEKK) joints: influence of process parameters and annealing on weld properties

Marcela Matus-Aguirre, Benoît Cosson, Christian Garnier, Fabrice Schmidt,  
Andre Chateau Akue Asseko, France Chabert

### ► To cite this version:

Marcela Matus-Aguirre, Benoît Cosson, Christian Garnier, Fabrice Schmidt, Andre Chateau Akue Asseko, et al.. Characterization and modeling of laser transmission welded polyetherketoneketone (PEKK) joints: influence of process parameters and annealing on weld properties. *Journal of Advanced Joining Processes*, 2024, 10, pp.100252. 10.1016/j.jajp.2024.100252 . hal-04697243

**HAL Id: hal-04697243**

**<https://imt-mines-albi.hal.science/hal-04697243v1>**

Submitted on 16 Sep 2024

**HAL** is a multi-disciplinary open access archive for the deposit and dissemination of scientific research documents, whether they are published or not. The documents may come from teaching and research institutions in France or abroad, or from public or private research centers.

L'archive ouverte pluridisciplinaire **HAL**, est destinée au dépôt et à la diffusion de documents scientifiques de niveau recherche, publiés ou non, émanant des établissements d'enseignement et de recherche français ou étrangers, des laboratoires publics ou privés.



Distributed under a Creative Commons Attribution 4.0 International License



## Characterization and modeling of laser transmission welded polyetherketoneketone (PEKK) joints: Influence of process parameters and annealing on weld properties

Marcela Matus-Aguirre<sup>a,b,c</sup>, Benoît Cosson<sup>\*a,b</sup>, Christian Garnier<sup>a</sup>, Fabrice Schmidt<sup>c</sup>, André Chateau Akué-Asséko<sup>b</sup>, France Chabert<sup>a</sup>

<sup>a</sup> Laboratoire Génie de Production, Université de Technologie Tarbes Occitanie Pyrénées, University of Toulouse, Tarbes, Tarbes 65000, France

<sup>b</sup> Centre for Materials and Processes, IMT Nord Europe, Institut Mines Télécom, University of Lille, Lille F-59653 Villeneuve d'Ascq, France

<sup>c</sup> Institut Clement Ader, IMT Mines Albi-Carmaux, Institut Mines Télécom, University of Toulouse, Albi 81013, France

### ARTICLE INFO

#### Keywords:

Plastic welding  
Laser transmission welding  
Weld joint morphology  
Polymer crystallinity  
Single-lap shear tests

### ABSTRACT

Welding high-performance thermoplastics has gained popularity across various industries such as automotive, aerospace, and medical. Laser transmission welding (LTW) has emerged as an effective method for joining thermoplastic parts due to its precise control and high joint quality. PAEK (polyaryletherketone) are wide spreading over various industrial applications as a substitute to metals and thermosets when high durability and performance are required. Polyetherketoneketone (PEKK) is one of these PAEK and it has received less attention than PEEK until now. PEKK, being a semi-crystalline thermoplastic, requires additional care during processing due to its propensity to crystallize. This study presents both experimental and numerical investigations into LTW of PEKK molded parts, aiming to understand the influence of welding parameters and crystallinity on weld joint morphology and mechanical properties. PEKK plates, prepared in amorphous and semi-crystalline states, are subjected to LTW using a 975 nm diode laser. Material characterization confirms differences in crystallinity between the samples, which affect their thermal and optical properties, which are crucial for welding. Welding tests are conducted with varying laser power (between 75 and 95 W) and semi-transparent part thickness (2 and 4 mm). The morphology of joints is analysed. Assemblies undergo post-weld annealing treatment to examine its influence on weld crystallinity and consequent mechanical properties. Results reveal an anisotropic distribution of crystallinity within the heat-affected zone (HAZ). The depths of the molten layer (ML) and semi-crystalline layer (scL) vary with laser power and assembly type. A notable decrease in weld strength with laser power is highlighted, while annealing leads to enhanced crystallinity and improved weld strength. Despite variations, high weld strengths are achieved with annealing. Computational modelling elucidates the complex interplay between laser irradiation, temperature distribution, and crystallization kinetics observed experimentally. Overall, this comprehensive investigation provides valuable insights into optimizing LTW parameters for PEKK parts.

### Introduction

In recent years, welding has been considered as a promising technique for assembling high-performance plastics and composites. This trend is driven by the growing demand of such lightweight materials in high-demanding industries such as aerospace and medical device manufacturing. Welding high-performance thermoplastics (TP) and TP matrix-based composites bring new challenges to be overcome, due to

their higher melting temperature, sensitivity to thermo-oxidative degradation and hydrolysis compared to conventional thermoplastics. Moreover, some high-performance thermoplastics such as polyaryletherketones (PAEK) require additional care when processed due to their ability to crystallize.

To date, only a few research works demonstrate the weldability of PAEK, particularly for the polyetheretherketone (PEEK) material (Ahmed et al., 2018; Carassus et al., 2023; Dubé et al., 2015; Flanagan

\* Corresponding author at: Laboratoire Génie de Production, Université de Technologie Tarbes Occitanie Pyrénées, University of Toulouse, Tarbes, Tarbes 65000, France.

E-mail address: [benoit.cosson@uttop.fr](mailto:benoit.cosson@uttop.fr) (B. Cosson).

<https://doi.org/10.1016/j.jajp.2024.100252>

Received 20 April 2024; Received in revised form 4 June 2024; Accepted 5 September 2024

Available online 10 September 2024

2666-3309/© 2024 The Author(s). Published by Elsevier B.V. This is an open access article under the CC BY license (<http://creativecommons.org/licenses/by/4.0/>).

et al., 2018; González et al., 2014; Jose and Panneerselvam, 2021; Korycki et al., 2023; Kosloh et al., 2017; Ma et al., 2020). Welding other PAEK is barely studied, due to the novelty of such polymers compared to PEEK. Among the PAEK thermoplastics, polyetherketoneketone (PEKK) stands out for its outstanding performance in demanding applications. Indeed, the commercialization of PEKK has grown for about fifteen years ago. PEKK, being a high-performance semi-crystalline thermoplastic polymer, has an exceptional resistance to extreme environments, like those in aerospace and oil exploration (France, 2024). Its melting point is one of the highest among thermoplastics, 300 °C to 360 °C depending on the grade, and provides excellent resistance to chemicals and abrasion. Joining PEKK and PEKK-based composites parts have been proved by some welding process such as induction (Grouve et al., 2020; Jeong et al., 2023; Kwon et al., 2021; Modi et al., 2023), resistance (Dubé et al., 2015; 2008; 2012; Russello et al., 2023; Shi et al., 2013), and ultrasonic (Broek, 2015; Köhler et al., 2021; Mongan et al., 2022). Despite these convincing research works, the transfer to real industrial cases is still in its infancy. The limitation is mainly due to the lack of repeatability of weld properties. Among the available processes, laser transmission welding (LTW) is a promising technology due to short time cycles and dimensional accuracy.

In LTW, two overlapped thermoplastic parts are welded using a near-infrared (NIR) laser beam. Conventional LTW requires the upper part to be semi-transparent to the laser wavelength, while the lower part must absorb the laser energy. Therefore, the laser beam goes through the upper part and irradiates the assembly interface. Here, the laser energy is concentrated thanks to the absorbent properties of the lower part. By heat conduction, both parts are heated at the interface and the macromolecules move and diffuse from one part to the other. This macromolecular diffusion occurs when the temperature exceeds the glass transition ( $T_g$ ) of the polymer in case of amorphous thermoplastics. In contrast, when working with semi-crystalline polymers, higher energy levels are required to reach their melting temperature ( $T_m$ ).

The optical properties of the materials are thus crucial for LTW to be achieved. Most thermoplastics are semi-transparent to the NIR laser irradiation in their natural state (Acherjee, 2020; Gonçalves et al., 2021). When assembling two polymers by LTW, the lower part is rendered absorbent with additives, like colorants (Amanat et al., 2011; Chabert et al., 2020) or fibers (Korycki et al., 2022; Pereira et al., 2019), to achieve energy absorption at the interface. An innovative option is to tune the crystallinity of the material to obtain a semi-transparent part and an absorbent one with the same polymer. This is only possible with a few thermoplastics for which the crystallization kinetics can be controlled. PEKK has this ability to be easily obtained in amorphous state by rapid cooling from the melting and semi-crystalline state by slow cooling from high temperatures.

The welding of amorphous PEKK on crystallized PEKK has been successfully achieved in previous studies (Matus Aguirre, 2023; Villar et al., 2018) without the need of any additive that could potentially contaminate the parts and impact the weld properties. In Villar et al. (2018), focus was put on characterizing the temperature distribution along the assembly thickness during LTW to optimize the process parameters. While in Matus Aguirre (2023), the effect of materials properties and process parameters on the weld joint quality was studied. However, despite these initial findings, a deeper understanding of the link between the generated weld joint morphology, material crystallinity, and mechanical resistance is essential to ensure repeatability and improve weld reliability. Additionally, qualitative validation of the welding process's effect on weld joint morphology through numerical simulations is essential for extensive understanding and optimization of the process.

The present work studies the weld joints obtained by assembling amorphous and semi-crystalline PEKK by laser transmission welding with a 975 nm diode laser. The properties of the PEKK samples are described to explain the influence of crystallinity on their thermal and optical properties. For welding, laser power and semi-transparent part

thickness are varied and correlated with the morphological and mechanical properties of weld joints. The LTW process generates a non-homogeneous heat affected zone (HAZ) within the weld joint in terms of crystallinity. This crystallinity gradient leads to various fracture mechanisms. As an attempt to homogenize the crystallinity throughout the joints, subsequent annealing is conducted on some assemblies. The aim is to assess the influence of the weld joint crystallinity on its mechanical properties. Additionally, numerical modelling of the welding process is developed in MatLab to predict the weld joint morphology and the whole thermal history in the PEKK assemblies, obtaining a favorable correlation with experimental observations.

## Materials and methods

### Material of study and samples production

Kepstan® polyetherketoneketone (PEKK) grade 7002 is provided by Arkema France in pellets. PEKK is a high-performance semi-crystalline thermoplastic of the poly-aryletherketone (PAEK) family. PEKK is synthesized from diphenyl ether (DPE), and terephthalic (T) and isophthalic (I) acid moieties. Different grades of PEKK are commercially available depending on their T/I ratio: 60/40, 70/30 and 80/20 grades. The T/I ratio of PEKK modifies its thermal transitions, degree of crystallinity and crystallization kinetics (Gardner et al., 1992; Hsiao et al., 1994; Perez-Martin et al., 2021). PEKK 7002 with a T/I of 70/30 is chosen for the study. This grade of PEKK has a medium crystallization kinetics, which is slow enough for easy modification of its crystallinity based on processing parameters.

Plates of  $95 \times 95 \text{ mm}^2$  are injected from the pellets with an injection molding machine Proxima 50 from Billion. The plates are obtained in two different crystalline states: amorphous (PEKK-A) and semi-crystalline (PEKK-SC). The amorphous state is achieved by setting the mold temperature at 70 °C for a holding time of 30 s, whereas the semi-crystalline one is obtained at 240 °C for 2 min. The square plates are molded with a thickness of 2 and 4 mm for the amorphous state (PEKK-A2 and PEKK-A4, respectively), and in 2 mm thick for the PEKK-SC. The PEKK-A plates are yellow and translucent, while PEKK-SC are beige and opaque.

Before processing, the pellets are dried to reduce the moisture during the injection process. To choose the drying time, the drying of PEKK pellets is measured by measuring the weight loss with time. The pellets are dried at 120 °C, as indicated by the supplier (Arkema France, 2021), from 0 to 30 h, in an oven UFP400 from Memmert. Fig. 1 shows the moisture content % evolution in the PEKK pellets. After 6 h, PEKK pellets have lost 93 % of the initial water content. The weight is stable after 22 h of drying. Thus, PEKK pellets are dried at 120 °C for 30 h before further processing.

**Crystallinity and thermal transitions** Differential scanning calorimetry (DSC) is used to verify the differences in crystallinity between the injected samples and to characterize their thermal transitions. A DSC Stare System Mettler Toledo is used to conduct the tests. Samples weighing  $6 \pm 3 \text{ mg}$  are extracted from each PEKK plate and placed inside hermetic aluminum pans. Using ramps of  $10 \text{ K min}^{-1}$ , samples are heated from 100 °C to 390 °C, cooled from 390 °C to 100 °C, and then heated again from 100 °C to 390 °C under a  $50 \text{ mL min}^{-1}$  nitrogen flow. At the beginning of each test, samples are stabilized at 100 °C for 5 min, and there is no hold between the heating and cooling cycles.

Fig. 2 a shows a typical DSC thermogram of PEKK-A sample. On the first heating, glass transition temperature ( $T_g$ ), melting temperature ( $T_m$ ), and crystallinity ( $X_c$ ) are obtained for each sample. Cold crystallization temperature ( $T_{cc}$ ) is also obtained for the PEKK-A plates. The cooling ramp is used to obtain the crystallization temperature from melt ( $T_{cm}$ ) and the maximum crystallinity ( $X_{c-max}$ ) for the material. The second heating gives the maximum melting temperature after crystallization from the melt. Fig. 2b focus on the DSC scans from 150 to 250 °C

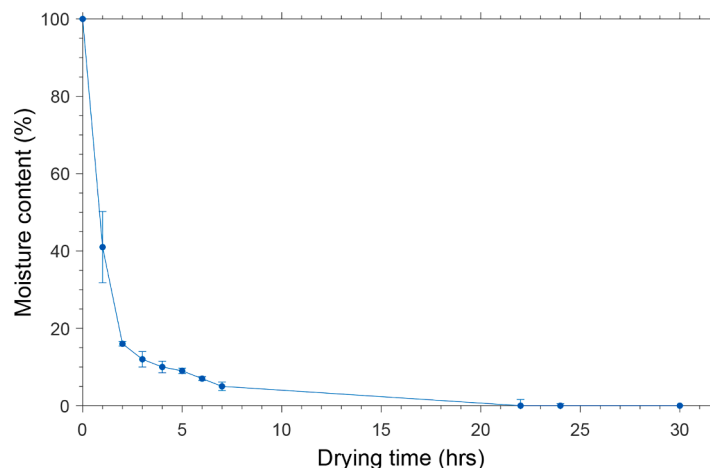


Fig. 1. Normalized weight loss during drying of PEKK pellets at 120 °C. Error bars indicate standard deviation.

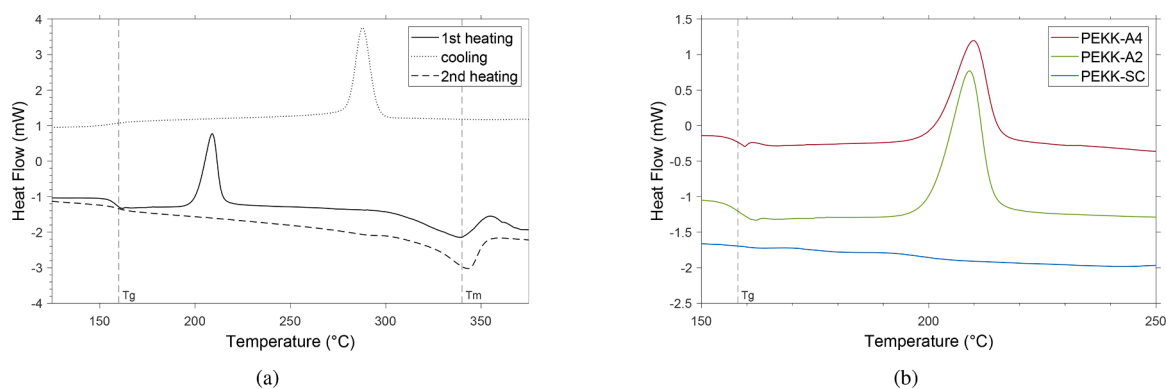


Fig. 2. (a) Typical DSC thermogram of PEKK-A samples. (b) Cold crystallization peaks of PEKK injected samples.

obtained on the first heating for each sample. After the glass transition ( $T_g$ ), an exothermic peak is observed around 205 °C for the amorphous samples (green and red curves). This indicates cold crystallization, occurring when the sample is not fully crystallized on cooling. Indeed, right after  $T_g$ , the macromolecules have gained enough mobility to self-organize into crystalline structures. For PEKK-SC, no peak is observed because the sample was fully crystallized during processing. The crystallinity of the samples is calculated thanks to Eq. (1) (Doumeng et al., 2021). The thermal transitions and crystallinity obtained from the DSC tests are summarized in Table 1.

$$X_c = \frac{\Delta H_m - \Delta H_{cc}}{\Delta H_{100\%}} \quad (1)$$

The enthalpy of the cold crystallization peak ( $\Delta H_{cc}$ ) is subtracted from the melting enthalpy of the first heating ( $\Delta H_{mc}$ ). The result is then divided by the theoretical enthalpy of the 100 % crystallized polymer ( $\Delta H_{100\%}$ ). This last enthalpy is unknown for PEKK, so is commonly assumed to be the same as for PEEK ( $130 \text{ J g}^{-1}$ ) (Blundell and Osborn,

1983). For the enthalpy calculation, the correspondent peaks are integrated with a *spline* baseline.

**Optical properties** The optical properties of the samples in NIR light are important for laser transmission welding. The laser intensity that strokes the surface of the sample can be transmitted, reflected and/or absorbed. The differences in crystallinity induce an effect on optical properties. This is evident in visible light: PEKK-A plates are transparent with a yellow coloration, whereas PEKK-SC plates are matte, with a beige coloration. The transparency of the sample at the Near-infrared (NIR) light of a laser beam can be different than at the visible light. The majority of polymers are semi-transparent or translucent under visible and near-infrared (NIR) wavelengths in their natural state (Acherjee, 2020; Gonçalves et al., 2021; Xu et al., 2015a). Nevertheless, the optical properties of semi-crystalline polymers are influenced by their crystalline structure, which imposes limitations on light transmission (Kagan and Bray, 2001). The crystalline structure increases the light travel path, which leads to higher absorption (Kagan et al., 2002; Xu et al., 2015b).

A FTIR spectrophotometer Bruker Vertex 70 is used to measure optical properties of the injected plates. Transmission ( $T_i$ ) and reflection ( $R_i$ ) factors are measured using an integration sphere with an Infragold Lambertian coating. Characterization is made at room temperature for the wavelength range of 0.9 to 2  $\mu\text{m}$ . Absorption factors ( $A_i$ ) are obtained using Eq. (2) (Mamuschkin et al., 2014), according to the energy conservation principle. The optical properties of the samples at the wavelength of interest (975 nm cf. section 2.2) are summarized in Table 2.

$$T_i + R_i + A_i = 1 \quad (2)$$

Table 1  
PEKK injected plates thermal transitions, crystallinity, coloration and thickness.

PEKK	A2	A4	SC
$T_g$ [°C]	151	152	160
$T_{cc}$ [°C]	204	205	–
$T_m$ [°C]	337	336	338
$T_{cm}$ [°C]	285	286	284
$X_c$ [%]	5	6	24
Thick [mm]	2	4	2
Color	Yellow	Yellow	Beige/White

**Table 2**  
Optical properties of PEKK samples at the laser wavelength of interest (975 nm).

PEKK	A2	A4	SC
$T_i$ %	75	62	20
$R_i$ %	13	13	48
$A_i$ %	12	25	32

The transmission spectra of PEKK samples are seen in Fig. 3 (top). As expected, the transmittivity of amorphous samples is higher than those of the semi-crystalline ones. Also, it can be noticed how the transmission decreases when increasing the PEKK-A thickness from 2 to 4 mm. At the wavelength of interest of 975 nm, PEKK-A2 has the highest transmission factor of 75 %, followed by PEKK-A4 with 62 %. Previous works of LTW of PEKK (Villar et al., 2018) indicated that a transmission factor of 60 % is high enough to achieve irradiation and melting at the interface of the assembly. Thus, the transmission factors obtained in PEKK-A samples validate their suitability as upper-semi-transparent parts for LTW process. Meanwhile, the transmission factor of PEKK-SC is 20 % at 975 nm.

Fig. 3 (middle) shows the reflection spectra of PEKK samples. A correction factor of 0.94 is applied to the measured reflection to take into account the reflectivity of the integration sphere. Contrary to the transmission, the reflection decreases with crystallinity. The reflection properties of a thermoplastic are significantly impacted by its crystallinity. Xu et al. (2015a) found that higher crystallinity is associated with an augmented apparent reflection, attributed to an increase of back-scattering. Also, the thickness of the amorphous samples does not modify their reflection properties. As observed by Coelho et al. on PE and PP films, the reflectance remained approximately constant for the different thicknesses studied (Coelho et al., 2004).

The absorption spectra are obtained from the measurements of transmission and reflection, in Fig. 3 (bottom). The absorption factor increases with thickness and with the crystallinity. The absorption factors obtained at 975 nm are reported in Table. The samples with the highest absorption is PEKK-SC with 32 %, which is higher than its transmission factor of 20 %. As proven by Goyal et al. when welding transparent polycarbonate with an absorbent layer at the interface, an absorption factor of 30 % is high enough to achieve welding (Goyal and Kant, 2023). This validates the suitability of PEKK-SC as a lower-absorbent part for LTW.

To quantify the intrinsic properties of absorption of the samples at the wavelength of interest, the absorption coefficient  $\alpha$  [ $\text{m}^{-1}$ ] is calculated by using the Lambert-Beer's law Bachmann and Russek (2002) with Eq. (3):

$$I_T = I_o \exp(-\alpha \cdot z) \quad (3)$$

where  $I_T$  [ $\text{W m}^{-2}$ ] is the quantity of intensity that goes through the sample thickness,  $I_o$  [ $\text{W m}^{-2}$ ] is the quantity of energy that enters the material after stroking the surface of the sample, and  $z$  [ $\text{m}$ ] is the thickness of the sample. Using the corresponding values of  $T_i$  and  $R_i$  factors at 975 nm in the equation, the absorption coefficient is obtained for each sample, summarized in Table 3.

**Table 3**  
Absorption coefficient  $\alpha$  calculated for each sample.

PEKK	A2	A4	SC
$\alpha$ [ $\text{m}^{-1}$ ]	74.2	84.7	477.75

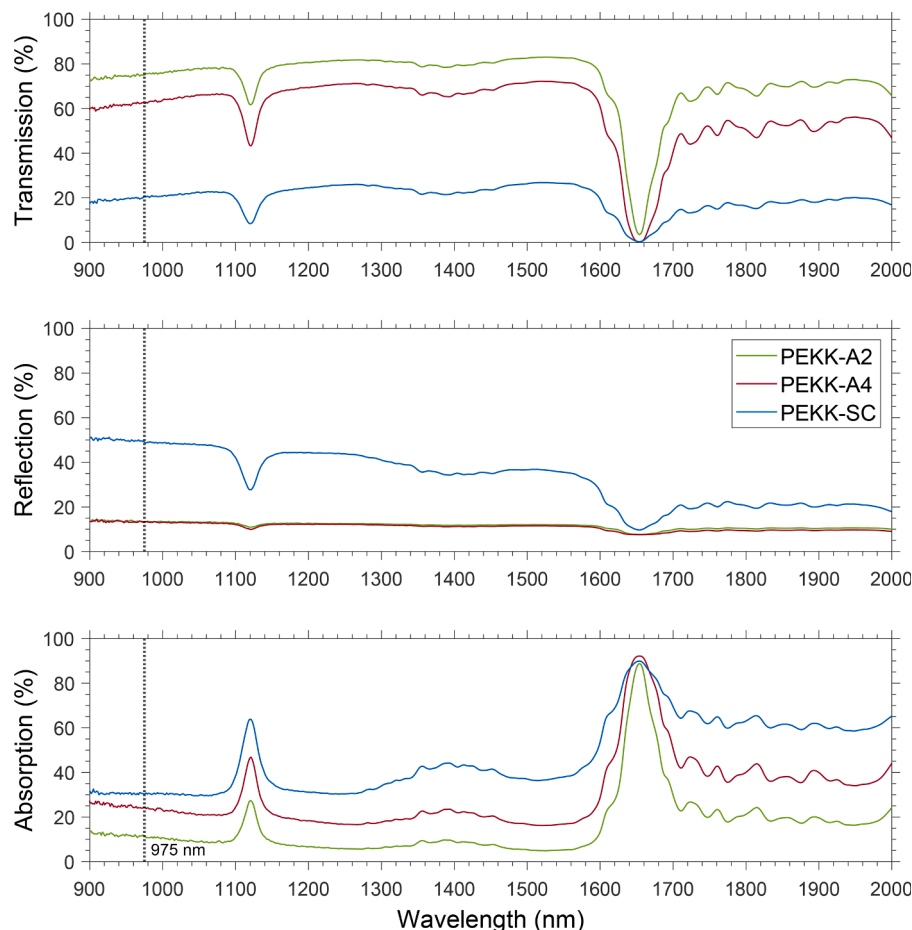


**Fig. 3.** Transmission, Reflection and Absorption spectra of PEKK injected plates.

**Thermal properties** The heat capacity  $C_p$  [ $\text{J kg}^{-1} \text{K}^{-1}$ ] of PEKK is measured by a DSC TA Instrument Q200. The heat conductivity  $k$  [ $\text{W m}^{-1} \text{K}^{-1}$ ] is obtained by Hot disk method using a TPS2500 from Hotdisk Instrument. The density  $\rho$  [ $\text{kg m}^{-3}$ ] of the material is given in the material's technical datasheet [Arkema France \(2021\)](#), and it is considered equal for all samples, regardless its crystallinity. All these properties are summarized in [Table 4](#).

### Welding tests

PEKK plates are cut into rectangular parts of 95 mm length by  $25 \pm 3$  mm width. The samples are dried at  $120^\circ \text{C}$  and kept in a desiccator until welding. Before welding, the samples' surfaces are cleaned with acetone.

A welding machine ES Weld 200 with a 975 nm diode laser and a Gaussian beam profile is used for welding. The output laser power can be adjusted between 0 and 200 Watts, with a precision of  $\pm 3$  W. A circular shape laser beam is used, with a 6 mm beam diameter, obtained at maximum laser defocus. Inside the machine, samples are positioned and held on the platform in a lap-joint configuration ([Fig. 4](#)). PEKK-A sample is positioned over the PEKK-SC one, with an overlap of 12.5 mm as indicated on ISO 4587:2003. Close contact between the samples is ensured by applying a constant pressure of 3.8 MPa with a semi-transparent glass plate on the welding platform. The glass plate used for clamping has a transmissivity of 83 %. It is measured with a Gentec Pronto-500 powermeter, by comparing the output power measured before and after going through the glass plate.

A weld is created at the center of the overlap area from L0 to Lw, as shown by the red line in [Fig. 4](#). A specific welding procedure combining static and dynamic irradiation is used to achieve an uniform melting zone at the interface. The procedure begins with a static irradiation for 2 s at L0, then the laser moves forward at constant speed irradiating until Lw, to finish with a static irradiation of 1 s at Lw, before tuning off. The welding speed used for the dynamic irradiation is  $60 \text{ mm min}^{-1}$ . As determined by preliminary welding tests, this is the optimal welding speed to achieve melting at the interface, regardless of the laser power. Moreover, this welding speed is maintained constant for all welds made. After irradiation, the assembly is kept clamped for 120 s until cooling of the weld joint.

Two parameters are varied for the study: the thickness of the upper semi-transparent part and the laser power used to irradiate the assembly. Two different thicknesses are employed for the upper PEKK-A part, as indicated in [Fig. 4](#): 2 and 4 mm (referred as PEKK-A2 and PEKK-A4, respectively). The laser intensities are chosen from the power-range that allows melting at the interface without burning, that is between 75 and 95 W. This power-range was determined from previous laser-material interaction tests. To narrow the study, four laser power intensities were selected, based also on preliminary welding tests: 75, 85, 88 and 95 Watts. Amanat et al. studied the welding process of PEEK-injected plates of 0.7 mm thickness [Amanat et al. \(2011\)](#) they found that laser power is a crucial parameter for weld strength, whereas irradiation time has little effect. Other works on PEEK and their composites, have also focused on laser power [Korycki et al. \(2022\)](#); [Liu et al. \(2022\)](#).

Each upper part (2 and 4 mm) is paired with the lower absorbent PEKK-SC part, resulting in two types of assemblies: PEKK-A2/SC and PEKK-A4/SC. These assemblies are welded using four laser powers to obtain 8 assembly combinations, as detailed in [Table 5](#).

**Table 4**

Thermal properties of PEKK samples.

PEKK	A	SC
$k$ [ $\text{W m}^{-1} \text{K}^{-1}$ ]	0.246	0.211
$C_p$ [ $\text{J kg}^{-1} \text{K}^{-1}$ ]	973	1138
$\rho$ [ $\text{kg m}^{-3}$ ]	1290	1290

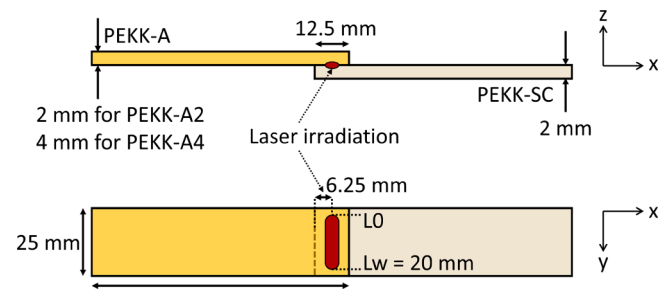


**Fig. 4.** Lap-joint configuration for welding PEKK-A/PEKK-SC. Schematic diagram not to scale.

**Table 5**

Assembly combinations for the study.

Laser power	75 W	85 W	88 W	95 W
PEKK-A2/SC	A2/SC-P1	A2/SC-P2	A2/SC-P3	A2/SC-P4
PEKK-A4/SC	A4/SC-P1	A4/SC-P2	A4/SC-P3	A4/SC-P4

### Annealing of welds

An annealing treatment is carried out on some of the assemblies to increase the crystallinity of the welded zone. Annealing is performed at  $190^\circ \text{C}$  for 3 h. The welded assemblies are placed into a mold to avoid sample deformation and placed inside an oven UFP400 from Memmert. The mold is pre-heated in the oven at the annealing temperature. After annealing, the assemblies are slowly cooled inside the mold up to room temperature. Then, they are stored in a desiccator before further testing.

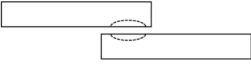
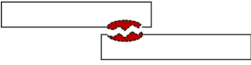
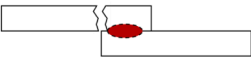
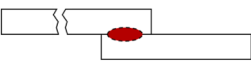
### Weld joint characterization methods

The lap-joint assemblies are characterized by single lap shear (SLS) tests. A tensile machine INSTRON 550R is used with a load cell of 50 kN and a cross-head load rate of  $2800 \text{ N min}^{-1}$ . Eight assemblies are tested for each parameter for the PEKK-A/SC non-annealed welds. Three samples are tested per parameter for the annealed assemblies. All the assemblies are tested until failure. After failure, samples are inspected to identify the failure type. Failure type is selected from standard definitions established in previous work [Matus Aguirre \(2023\)](#) and shown in [Table 6](#). Within the PEKK assemblies, two main failure types are observed: the Cohesive (CI) and the Substrate Near Joint (SNJ). When the assembly fails in CI type, it means that the assembly separates by shear at the interface within the weld joint. In-plan shear failure mode is achieved, which is the failure mode that gives the real weld strength. The SNJ failure indicates that the bulk sample breaks near the weld joint heat-affected zone (HAZ). This suggests that the assembly failed by tensile mode within the bulk.

The force at failure ( $F_f$ ) is thus recorded for each assembly, regardless the failure type. For the assemblies that failed in CI type, the  $F_f$  corresponded to the force at which the assembly separated at the interface within the joint. For SNJ failure type, the  $F_f$  is the one obtained when one of the bulk samples breaks near the weld joint. To quantify the mechanical results, the force at failure ( $F_f$ ) is considered to calculate the weld strength. Two types of stresses are calculated, the failure stress ( $\sigma_f$ ) and the lap shear stress (LSS). For both, the ( $F_f$ ) is divided by the contact area ( $A_c$ ). The  $A_c$  is different for each stress, depending on the zone where the failure occurred.

Numerical optical microscope VHX-6000S from Keyence is used to visualize the weld joint. The assemblies are observed to characterize the weld joint cross-section along the weld path. These weld cross-sections are cut, embedded in an epoxy resin, and polished before microscopy observations. The post-failed CI-type assemblies are characterized at the separation zone (the irradiated interface) to study their failure zones.

**Table 6**  
Failure types definitions from Matus Aguirre (2023).

Failure type	Appearance	Inference	Description
Interfacial		Bond strength $\ll$ substrate strength	Assembly fails at the interface because no real material cohesion was created at the irradiated interface. Most undesired result.
Cohesive		Bond strength $\sim$ substrate strength	Assembly fails at the interface within the weld bond created.
Substrate near joint (SNJ)		Bond strength $>$ substrate strength	Failure within the substrate but near the interfacial region and weld bond intact (or mostly).
Bulk substrate		Bond strength $\gg$ substrate strength	Bulk substrate results in tensile yield and breaks far from the weld bond. Most desired result.

### Model of LTW

The geometry of the model is defined in the 3D space  $(x, y, z)$ . Only the overlap area of  $25 \times 12.5 \text{ mm}^2$  with the corresponding thickness of each sample, is modeled to restrict the calculation time. A meshgrid is generated with the discretization of the geometry for each direction in the 3D space. The length  $L_x$  of the model goes from 0 to 25 mm with a spatial step  $dx = 0.0002 \text{ [m]}$  in X. Its width  $w_y$  goes from 0 to 12.5 mm, with a spatial step  $dy = 0.0002 \text{ [m]}$  in Y. The thickness  $th_z$  of the model goes from -2 mm (the thickness of PEKK-SC sample) to 2 mm (thickness of PEKK-A2 sample) with a spatial step of  $dz = 0.0001 \text{ [m]}$  in Z. The chosen spatial steps ensure both good convergence and an accurate representation of the temperature gradient resulting from laser irradiation.

The Gaussian shape of the laser beam is used and the irradiation is applied with a movement in the X axis. Irradiation is modeled with a starting point at  $X = 2.5 \text{ mm}$  and an ending point at  $X = 22.5 \text{ mm}$ , to create a weld path length of 20 mm, as for the experimental welding tests.

The thermo-optical and crystallinity models are solved thanks to finite difference method using an Eulerian time integration scheme with a time step  $dt = 0.002 \text{ [s]}$ .

### Thermo-optical model

The laser transmission welding process involves thermodynamic phenomena caused by the laser irradiation. The model is defined based on the heat transfer that occurs in the process. The heat balance Eq. (4) Cosson et al. (2009), with the mass conservation, is solved in MatLab:

$$\rho C_p \frac{\delta T}{\delta t} = \nabla(k \cdot \nabla T) + Q(r) \quad (4)$$

where  $\rho \text{ [kg m}^{-3}\text{]}$  is the density,  $C_p \text{ [J kg}^{-1} \text{ K}^{-1}\text{]}$  is the heat capacity and  $k \text{ [W m}^{-1} \text{ K}^{-1}\text{]}$  is the thermal conductivity of PEKK. Those parameters are given in Table 4. For the heat capacity, a function was implemented to model the changing phase from solid to melted, having a high peak of  $C_p$  at the melting temperature, shown in Eq. (5):

$$C_p = 20000 \frac{1}{\sigma_T \sqrt{2\pi}} \left[ \exp \left( -\frac{(T - T_m)^2}{2\sigma_T^2} \right) \right] + C_{p0} \quad (5)$$

$$C_p(T > T_m) = C_{p0}$$

with  $C_{p0}$  being the  $C_p$  of the PEKK-SC sample from Table 4, and  $\sigma_T = 6$ .

The source term  $Q \text{ [W m}^{-3}\text{]}$  in Eq. (4) represents the heat generated by the material due to the absorption of the laser radiation throughout its thickness, and is modeled by Eq. (6) Coelho et al. (2003):

$$Q(x, y, z, t) = \alpha I(x, y, t) \cdot \exp(-\alpha \cdot z) \quad (6)$$

where  $\alpha$  and  $z$  are respectively the absorption coefficient and the spacial position. The absorption coefficient  $\alpha$  is used as function of the crystallinity  $X_c$  of the samples. To obtain this correlation, the coefficients calculated in section 2.1 are used to make a linear interpolation and determine the parameter of the linear function for  $\alpha(X_c)$  (Eq. (7)).

$$\alpha(X_c) = \begin{cases} aX_c + b & \text{if } X_c > b/a \\ 0 & \text{if } X_c \leq b/a \end{cases} \quad (7)$$

Using the absorption coefficients of the PEKK samples that share the same thickness (PEKK-A2 and PEKK-SC), the parameters of the Eq. (7) are  $a = 2124$  and  $b = -11$ . When the materials are heated over the melting temperature ( $T_m$ ) they fully melt and all the crystals are vanished. Thus, when the temperature rises above  $T_m$ ,  $X_c$  is near zero (Eq. (8)). In this case, according to the parameters of Eq. (7) of  $\alpha(X_c)$ , if  $X_c \leq b/a$ ,  $\alpha$  can be negative. To avoid a negative value of  $\alpha$ , a condition is applied to  $\alpha$  so it became null if the temperature rises above  $T_m$ .

$$X_c(T > T_m) = \frac{b}{a} \quad (8)$$

The laser intensity  $I(x, y, t)$  is the initial intensity of the laser beam, which depends on the type of laser profile. In this study, a Gaussian laser beam is used.  $I(x, y, t)$  is thus calculated with Eq. (9):

$$I(x, y, t) = \frac{P}{2\pi \cdot \sigma^2} \exp \left[ \frac{-(x^2 + y^2)}{2\sigma^2} \right] \quad (9)$$

where  $P \text{ [W]}$  is the laser beam power that enters at the upper sample, and  $\sigma$  is the third of the laser beam radius.  $x$  and  $y$  are the spatial coordinates.

The heat equation is solved using the finite differential method, and  $Q(r)$  is calculated for all the volume of the sample of the assembly.

Dirichlet boundary conditions are used in the model. The temperature of the upper and lower part of the model are fixed at ambient temperature ( $18 \text{ }^\circ\text{C}$ ) for all the calculations.

### Crystallization model

To model the evolution of the crystallinity  $X_c$  due to the laser beam

irradiation, a crystallization kinetic model was implemented. The evolution of  $X_c$  was predicted as function of time and temperature with a model developed by Choupin et al. (2018) from the derivative of the Hillier model. The model developed by Choupin predicts the non-isothermal crystallization of PEKK 7002, and is shown in Eq. (10).

$$\frac{dX_R}{dt} = w_1 n_1 K_1 n_1^{\frac{1}{n_1}} \{ -\ln[1 - X_1(t)] \}^{\frac{n_1-1}{n_1}} [1 - X_1(t)] + w_2 n_2 K_2 [X_1(t) - X_2(t)] \quad (10)$$

where  $w_1$  and  $w_2$  are the weight factors of the primary and secondary crystallization in the relative crystallinity  $X_R$  of the material. Therefore,  $w_1 + w_2 = 1$ , corresponding to the Avrami model hypotheses that the relative crystallinity at infinite time is unity. The values of  $w_1$  and  $w_2$  calculated by Choupin et al. (2018) are indicated in Table 7.

As determined by Choupin for PEKK 7002 Choupin et al. (2018), the Avrami exponent for the primary crystallization  $n_1$  is equal to 3, which corresponds to a three dimensional growth with an instantaneous nucleation. For the secondary crystallization,  $n_2 = 1$ . This corresponds to a one dimensional crystallization growth with an instantaneous nucleation.

The Hillier crystallization rate constants  $K_1$  and  $K_2$  are expressed by the Hoffmann and Lauritzen theory of crystal growth. Therefore, the primary rate constant is:

$$K_1(T) = K_{01} \exp\left[\frac{-3U^*}{R(T - T_\infty)}\right] \exp\left[\frac{-3K_{g1}}{T\Delta T f}\right] \quad (11)$$

And, the secondary crystallization rate constant is:

$$K_2(T) = K_{02} \exp\left[\frac{-U^*}{R(T - T_\infty)}\right] \exp\left[\frac{-K_{g2}}{T\Delta T f}\right] \quad (12)$$

with the pre-exponential factors  $K_{01} = \frac{4}{3}\pi N_{01} G_{01}^3$  and  $K_{02} = N_{02} G_{02}$  independent of temperature. The first exponential term contains the contribution of the diffusion process to the growth rate, where  $U^*$  is the activation energy of the molecular transferring through the melt crystal interface,  $T_\infty$  is the temperature below which diffusion stops ( $T_\infty = T_g - 30$  K) with  $T_g = 160$  °C and  $R$  is the gas constant ( $8.314$  J mol<sup>-1</sup> K<sup>-1</sup>).

The second exponential term is the contribution of the nucleation process, where  $K_{gi}$  is the activation energy of nucleation for a crystal with a critical size,  $\Delta T$  is the degree of supercooling ( $\Delta T = T_{m0} - T$ ) with  $T_{m0}$  the equilibrium melting temperature and  $f$  is a correction coefficient for the temperature dependence of the melting enthalpy ( $f = 2T/(T_{m0} + T)$ ). The index  $i$  for  $K_{gi}$  is equal to 1 for the primary crystallization and 2 for the secondary crystallization. All the last mentioned parameters are given in Table 7.

The model shown in Eq. (10) calculate the relative crystallinity  $X_R$  of the material. To calculate the real crystallinity  $X_c$ , the  $X_R$  is multiplied by the maximum crystallinity possible to achieve the material  $X_\infty$ . In the case of PEKK  $X_\infty = 30$  %. Thus, Eq. (13) gives the final calculation of the crystallinity evolution in our material:

$$\frac{dX_c}{dt} = \frac{dX_R}{dt} X_\infty \quad (13)$$

## Results and discussions

### Weld joint morphology

The welds obtained from PEKK-A/SC assemblies are shown in Fig. 5. The weld joint cross-section along the weld path is visible for each assembly combination before and after welding. Prior welding, the interface line is easily noticeable between the overlapped samples. Then, for each power used for welding, a heat-affected zone (HAZ) is developed at the location of the previous interface line. All the cuts exhibit a similar HAZ: an oval shape with a color gradient from yellow to white, transitioning from bottom to top. As it can be noticed, a portion of the PEKK-SC bottom sample has now turned yellow. On the other hand, the PEKK-A top sample has acquired a white coloration at the top of the developed HAZ. These color changes on the samples suggest a modification on their crystalline state at the weld joint HAZ. As a result, an anisotropic weld joint in terms of crystallinity is generated after welding.

Given that PEKK is a semi-crystalline thermoplastic, its initial polymer microstructure can be significantly altered during laser welding, as proven by Ghorbel et al. in the case of semi-crystalline PP polymers Ghorbel et al. (2009). The different thermal gradients that the material experiences at the welding process can modify the crystalline microstructure of the injected samples. In case of PEKK 7002, change in crystallinity is easy to be identified by the coloration of the material. By examining the HAZ obtained on the different assemblies, two principal zones can be identified in Fig., which can be related to the thermal history of the welding process.

Zone 1 is the yellow portion of the HAZ that has replaced the interface line existing prior to weld. The yellow coloration of this zone indicates low crystallinity, or an amorphous state, as observed in the PEKK-A sample with a comparable color. It can be inferred that, during the irradiation process, both parts underwent melting within this zone which allow the macromolecules to diffuse and entangle to develop the weld joint. Then, when cooling, the material did not crystallize due to the fast cooling rate compared to the crystallization kinetics of PEKK from the melt. Indeed, a slow cooling ramp, lower than  $40$  °C min<sup>-1</sup>, is necessary for PEKK 70/30 to crystallize from the melt Quiroga Cortés et al., 2016. As proven by Quiroga Cortés et al., 2016, when PEKK 70/30 crystallizes from the melt at high cooling rates ( $40$  °C min<sup>-1</sup>) it exhibits cold crystallization endotherms. It means that a partial crystallization occurs on cooling. The crystallinity of PEKK 70/30 decreases from 28 % to 15 % with increasing the cooling rate from 10 to 40 °C min<sup>-1</sup>. Therefore, the crystallinity change after LTW process has already been proven by Liu et al. on PEEK/CFR-PEEK thin films. They correlated the crystallinity of the weld joint with the laser power Liu et al. (2022). Their results reveal a reduction of the crystallinity with the rapid cooling rate of the welding process. Zone 1 can also be considered as the "molten layer" (ML) of the HAZ.

Zone 2 of the weld joint HAZ is represented by the white portion developed over zone 1, inside the bulk PEKK-A sample. This white coloration indicates material cold crystallization. In this zone, a high temperature was achieved by thermal conduction of the interface irradiation. It can be inferred that the maximum temperature reached was between  $T_g$  and  $T_m$ , because the amorphous form of PEKK achieved to crystallize from the amorphous state. This is possible due to the fact that the molten layer (ML) generated is thick and the conductivity of the material is low, so the energy transferred by conduction from the ML to the bulk PEKK-A sample is stored for a long time, having enough time to crystallize. This zone 2 can also be called the "semi-crystalline layer" (scL) of the HAZ.

As illustrated in Fig. 6, it is obvious that the molten layer (ML)

**Table 7**  
Parameters for the crystallization kinetic model.

Parameter	PEKK 7002
$w_1$	0.78 (REF Choupin et al. (2018))
$w_2$	0.22 (REF Choupin et al. (2018))
$n_1$	3 (REF Choupin et al. (2018))
$n_2$	1 (REF Choupin et al. (2018))
$U^*$ [J mol <sup>-1</sup> ]	$4.9 \times 10^3$ (REF Choupin et al. (2018))
$K_{01}$ [min <sup>-3</sup> ]	$1.5 \times 10^{14}$ (REF Pérez-Martin et al. (2022))
$K_{g1}$ [K <sup>2</sup> ]	$5.041 \times 10^7$ (REF Pérez-Martin et al. (2022))
$K_{02}$ [min <sup>-3</sup> ]	$2.486 \times 10^5$ (REF Pérez-Martin et al. (2022))
$K_{g2}$ [K <sup>2</sup> ]	$2.025 \times 10^5$ (REF Pérez-Martin et al. (2022))

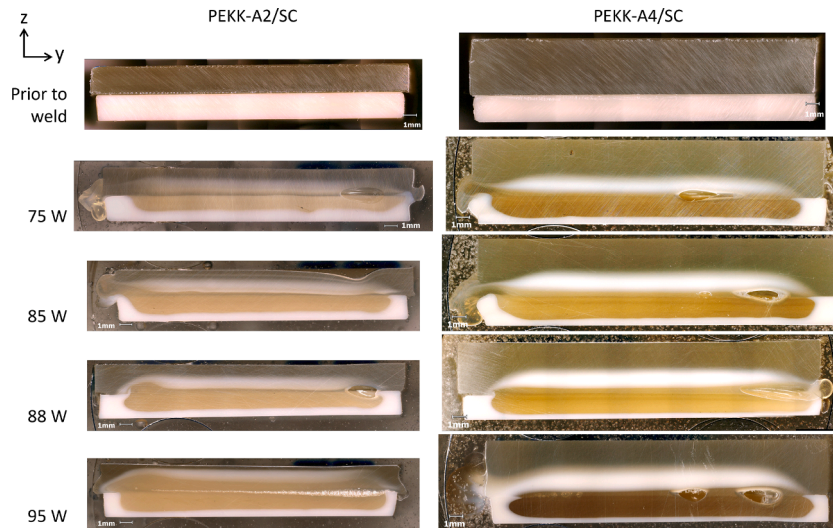


Fig. 5. Weld joints cross-sections along the weld path of the PEKK-A/SC assemblies. Representative micrographs for each assembly combination. The weld joint HAZ is recognizable as the oval shape with the color gradient.

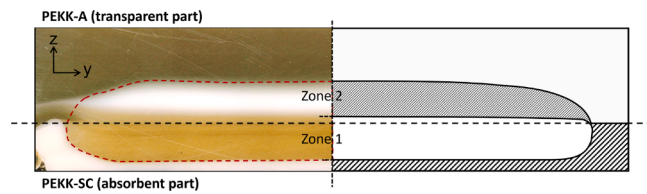


Fig. 6. Representative micrograph of the weld joint cross-section with a schematic representation of the different zones inside the weld joint HAZ. The interface location prior to weld is identified by the horizontal dotted line.

extends over both samples, although the depth of melting varies between them. The PEKK-A samples melted within a minimal depth, remaining close to the interface. The average depth of this ML on PEKK-A samples for both types of assemblies is  $0.4 \pm 0.1$  mm. On the other hand, the ML of PEKK-SC sample has a significant depth inside its thickness, nearly reaching the bottom of the substrate. This suggests that the laser irradiation penetrated the sample, as noted by Jones (2002), and was absorbed within the volume, rather than solely at the interface. The maximum depth that this ML achieves in the PEKK-SC sample is 1.6

mm for the A4/SC-P4 assembly. Welding substrates thinner than 1.6 mm would be tough with the parameters of this study. This asymmetric distribution of the ML was also observed on Abed et al.'s work when welding natural PP to PP pigmented with carbon black (Abed et al. (2001)). An asymmetric shape of the weld seam into the two materials was observed when the lower part is filled with a low pigment content (less than 1 %), resulting in low absorbing properties. They indicated that this allowed most of the energy to go deep inside the absorbing material, leading to a limited heat transfer to the upper part, obtaining moderated temperatures at the interface and lower dimensions of the melt pool. Even if the PEKK-SC sample melted with a significant depth in its thickness, it did not melt up to the bottom of the sample. The bottom of the PEKK-SC sample was in contact with the welding platform made of aluminum, which allows rapid heat dissipation.

Fig. 7 shows the HAZ layers (ML and scL) depth dimensions for each assembly combination. Focusing on the ML depths, a notorious increment of the molten depth is seen in both bulk samples when increasing the laser power. Inside the PEKK-SC sample the ML covers 53 % to 70 % of the original sample thickness of 2 mm when welded with PEKK-A2. When PEKK-SC is welded with PEKK-A4, this percentage increases, going from 74 % to 81 % of its thickness. On the other side, the melted

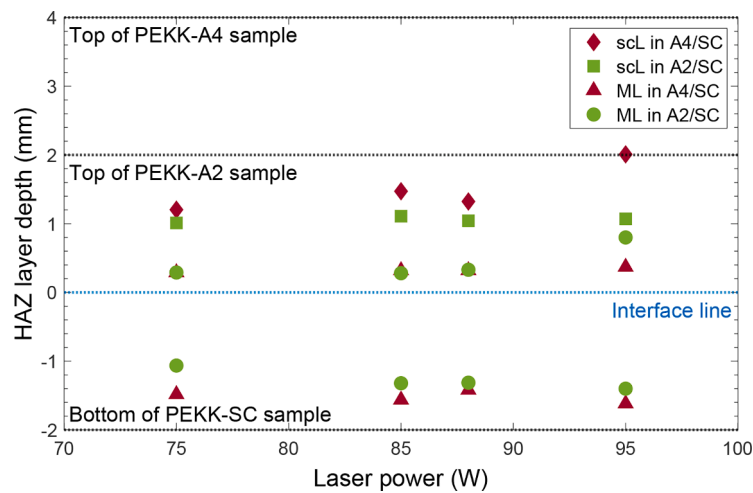


Fig. 7. Weld joint HAZ layers depths inside the thickness of each bulk sample for each assembly combination. (ML) indicate the molten layer, and (scL) the semi-crystalline layer. The values below the interface line indicate the ML depth in the PEKK-SC sample. The values above the interface line indicate the ML and scL depths on the PEKK-A samples.

layer in the PEKK-A sample is thin with almost the same dimensions for both types of assemblies. In the PEKK-A2 assemblies, the ML covers around 15 % of the original sample thickness when welding with P1, P2 and P3, and 40 % when using P4. In the PEKK-A4 samples, the thickness of the ML goes from 7 % to 9 % of the original thickness of 4 mm. As already proven by [Acherjee et al. \(2011, 2012\)](#) who studied LTW of PC, the molten depths in transparent and absorbing parts increase when increasing laser power and welding time. The increase in laser power results in greater heat input, leading to more molten material which generates larger weld dimensions.

The scL depth within the HAZ also exhibits a notable correlation with both laser power and assembly type, as seen in [Fig. 7](#). In the case of PEKK-A2/SC assemblies, the scL depth increases from 1.01 to 1.07 mm, covering more than 50 % of the thickness of the PEKK-A2 bulk sample. For PEKK-A4/SC assemblies, the scL depths increase from 1.2 to 2.01 mm, covering between 30 % and 50 % of the PEKK-A4 bulk sample thickness. Notably, only welding with the higher power value (P4) achieves a scL depth that covers 50 % of the PEKK-A4 sample thickness, while using lower laser powers yields scL depths that cover less than 37 % of the PEKK-A4 thickness. To date, no other study has documented the apparition or development of a scL within the HAZ over the ML, rendering it challenging to draw comparison with existing data.

The HAZ length is measured for each assembly combination and plotted with the power used for welding in [Fig. 8](#). The HAZ length is the maximum length measured along the Y axis inside the ML of the PEKK-SC sample. A notorious increment on the HAZ length with the power is noticed. This increment is almost linear for three of the four intensities (75, 85 and 95 W). The HAZ length obtained at 88 W do not follow the regular trend, that can be explained by the uncertainty of the power in the welding machine. Indeed, the values of power are defined with  $\pm 3$  %. Thus, the data obtained for 85 and 88 W are expected to be close to each other. Nevertheless, the increment of the HAZ length with laser power can be explained by the fact that increasing the laser power maximizes the heat input which leads to a greater volume of melted material at the interface, resulting in a higher welded zone. As it can be seen, the HAZ length of PEKK-A2/SC improves considerably with laser intensity, with a gap of 1.6 mm between the higher and lowest power. The HAZ length of PEKK-A4/SC assemblies also increases, but this increment is mainly notorious, with only 0.3 mm of difference from the lowest to the highest power, the HAZ length of these assemblies is quite the same. Moreover, this HAZ length is higher than the welding path used for welding (20 mm) in all the configurations. That indicates that the irradiation procedure used, combining static and dynamic irradiation, had a positive impact on the melting at the interface.

The HAZ length also increase with the increase of the transparent substrate thickness for each laser power. This can be caused by the

scattering of the laser irradiation through the samples. Thus, PEKK-A4 seems to scatter more the light than PEKK-A2, which increases the distribution of the energy over a longer area.

From [Fig. 5](#) it can be seen that most of the cross-sections show a void on the left side of their HAZ, near its end. This void was not caused by water evaporation, because samples were dried before welding, but mostly from flowing matter that escaped from the other side, as it can be clearly seen on the pictures. On the right side of the cross-section, outside the border, an extra of the material can be seen. This implies that the material that melted at the irradiation-welding process flowed from the interface line opposite to the welding trajectory.

**Crystallized assemblies** The annealing process aims to turn the amorphous state of the material to crystallization to its maximum degree. The effectiveness of annealing on promoting crystallization has already been proven by Liu et al. on PEEK/PEEK-CF LTW assemblies [Liu et al. \(2022\)](#). The annealing temperature must be between  $T_g$  and  $T_m$  to achieve crystallization in isothermal conditions from the amorphous state, as stands by [Quiroga Cortés et al., 2016](#). As seen in [Fig. 2a](#), PEKK-A crystallizes during the first heating ramp after the glass transition temperature. This crystallization is assessed by the exothermic peak after  $T_g$ , namely cold crystallization temperature ( $T_{cc}$ ). The crystallization of the amorphous form of the material starts with the development of the first germs. This first crystal germination occurs at the beginning of the exothermic peak when heating. The cold crystallization peak observed in [Fig. 2a](#) seems to start around 190 °C. Thus, this is the temperature established for the annealing process.

[Quiroga Cortés et al., 2016](#) investigated the impact of annealing on the physical structure of PEKK 60/40. They observed that prolonged annealing duration or annealing at higher temperatures led to a significant increase in crystallinity. They also associated the crystal improvement with the increment of the annealing time at a given temperature, resulting from conformational reorganizations during annealing. The annealing time is determined after several preliminary tests between 1 and 4 h. Thus, 3 h is the time used for annealing the assemblies.

The study of annealing is carried out on the following specimens: P2 (85 W) and P4 (95 W). These two powers are chosen from the results obtained in the mechanical characterization of PEKK-A/SC welds in section 3.2. Upon annealing, not only the weld joint is crystallized, but also the whole specimens. After crystallization, the assemblies are characterized visually and mechanically.

As it can be recalled, when welding PEKK-A/SC the weld joint obtained is non-homogeneous in terms of crystallinity, as it can be seen on [Fig. 9b](#). With the annealing process, crystallization is enhanced and a fully crystallized weld joint is obtained, as in [Fig. 9c](#). The cross-section of the weld joint shown on [Fig. 9c](#) has a more homogeneous color on its

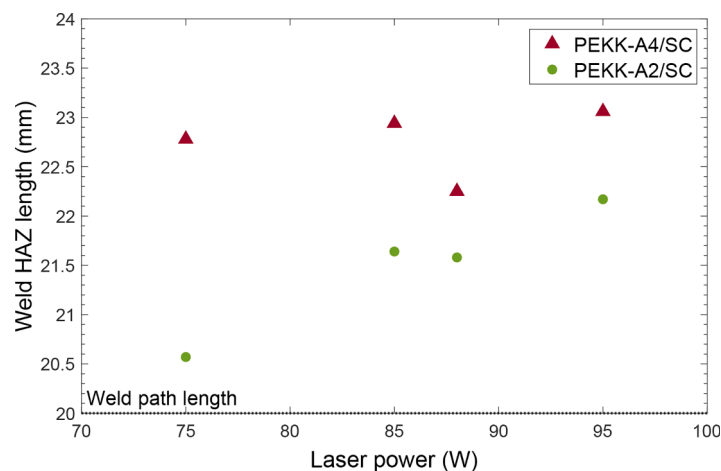


**Fig. 8.** Weld joint HAZ length plotted against laser power used for welding.

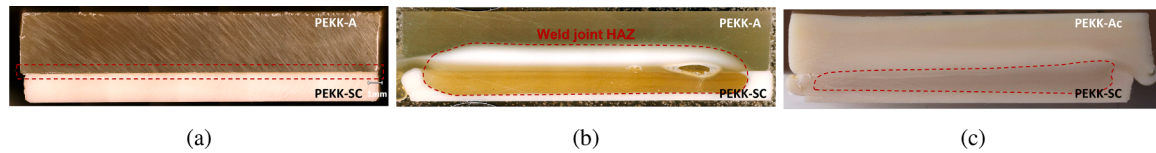


Fig. 9. PEKK-A/SC weld joint cross section a) before welding, b) after welding and c) after annealing process.

HAZ, compared to the HAZ obtained only after welding (Fig. 9b). Indeed, the full cross-section of the crystallized assembly shows only one coloration, which is beige. Having this color on the PEKK 70/30 samples indicates that the material has a high crystallinity. Thus, it can be inferred that the weld joint obtained after annealing is homogeneous in terms of crystallinity.

Although, as seen in Fig. 10, a darker region of beige coloration can be noticed on the crystallized weld cross-section for all assembly configurations. This darker region could be the amorphous zone (Zone 1) of the initial weld joint that crystallized during annealing. The crystallization generated gave a darker color because it was obtained from cold crystallization. It can be inferred that the crystalline structure obtained here is different from the PEKK-SC bulk sample. As already proven by different authors, PEKK exhibits two crystal polymorphisms (forms I and II) Gardner et al. (1994, 1992); Ho et al. (1994) that can develop depending on the crystallization conditions Cheng et al. (1996); Gardner et al. (1994); Ho et al. (1995, 1994). Gardner et al. suggested that under conditions of fast nucleation, such as cold crystallization with a significant degree of supercooling, form II is favored Gardner et al. (1994). They also identified that when PEKK 70/30 crystallizes from the cold, both forms I and II structures appear, contrary to crystallization from the melt which favor form I. This can indicate that the weld joints crystallized by annealing can have a mixture of forms I and II, thus the colors observed are darker than the PEKK-SC sample.

#### Weld joint mechanical properties

The results of the SLS mechanical tests are analysed in correlation with the welding parameters for the PEKK assemblies. Initially, the focus is placed on the non-crystallized (NC) assemblies, namely PEKK-A/SC. Fig. 11 shows the load at failure ( $F_f$ ) for all assembly combinations within the non-crystallized group. Notably, it is observed that the failure force increases when doubling the PEKK-A thickness for each power tested. Additionally, the breaking load increases with power for the first three power values, nearly doubling from 75 W to 88 W. For the PEKK-A2/SC assemblies, the load at failure escalates from 0.8 kN to 1.4 kN, representing an increment of 75 %. While for the PEKK-A4/SC assemblies, the force increases from 1 kN to 1.9 kN, marking a 90 % rise. However, at the highest power value, there is a subsequent decrement in the failure force, dropping by 21 % for the A2/SC, and 11 % for the A4/SC assemblies. The maximum failure force is thus recorded at 88 W of laser power, reaching 1.4 kN for A2/SC and 1.9 kN for A4/SC assemblies. These results are similar to those obtained by Goyal et al. when welding transparent polycarbonate samples of 2 mm thick with a fiber laser of 1080 nm wavelength Goyal and Kant (2023). In their work, the maximum breaking load of 1.18 kN was achieved at 100 W and a welding speed of 400 mm min<sup>-1</sup>.



Fig. 10. Weld joints cross-section along the weld path of the crystallized assemblies (PEKK-Ac/SC).

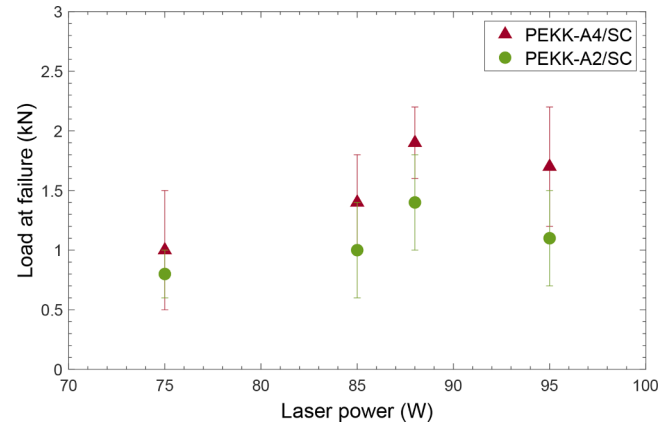


Fig. 11. Mechanical tests results showing the load at failure ( $F_f$ ) for all PEKK-A/SC assemblies combinations. Error bars indicate standard deviation.

As mentioned on section 2.4, two failure types were obtained within the PEKK assemblies: the CI and SNJ (refer to Table 6). A high percentage of the assemblies tested failed in substrate near joint (SNJ) type (see Table 6): 82 % for the PEKK-A2/SC, and 44 % for the PEKK-A4/SC. These assemblies failed within the bulk, really near the weld joint, they are thus considered as if the weld joint is stronger than the bulk material, as hypothesized by Amanat et al. (2010) when welding PEEK films. However, the failure stress  $\sigma_f$  can be calculated for the SNJ failed assemblies by dividing the  $F_f$  to the failure zone area  $A_f$ . The failed area is the section of the bulk sample that broke on the test. Fig. 12a shows the failure stress  $\sigma_f$  calculated for the assemblies that failed in SNJ type. The failure stress follows a similar tendency that the  $F_f$ , but, opposite to it, the  $\sigma_f$  is higher for the PEKK-A2/SC assemblies. This is because the PEKK-A2/SC assemblies have a smaller failure zone than the PEKK-A4/SC. Even if the PEKK-A2/SC assemblies failed within the amorphous or semi-crystalline bulk sample, their thickness is 2 mm. On the other side, the PEKK-A4/SC assemblies failed mostly in the amorphous sample, with a thickness of 4 mm. That means that the contact area that failed was higher, and even twice, of the area on the PEKK-A2/SC assemblies. And, to obtain a higher failure stress, the failure load should also be at least twice. But this was not the case, the failure force of the PEKK-A4/SC assemblies was just 47 % higher than the  $F_f$  of the PEKK-A2/SC assemblies.

CI type failure is achieved within a few assemblies: 18 % for the PEKK-A2/SC, and 64 % for the PEKK-A4/SC. When welding PEEK films with LTW, Amanat et al. obtained some CI failure in the crystalline group (only 38 %) Amanat et al. (2010). The CI failed weld joints are characterized by optical microscopy, as shown in Fig. 13. The HAZ of the weld joint is seen at the overlapped zone, the interface plane. This HAZ appears with a yellow coloration, as for Zone 1 of the weld joint defined in section 2.4. This indicates melting and change in the crystalline state of the PEKK-SC sample, becoming amorphous after welding. For each assembly combination, the weld joints show signs of sheared material. This indicates that the samples were melted and fused together at the irradiated zone and that the bonds were sheared during test, confirming a continuous material at the weld joint in the assembly by optical microscopy and used to calculate the real lap-shear-strength (LSS) of the CI failed assemblies.

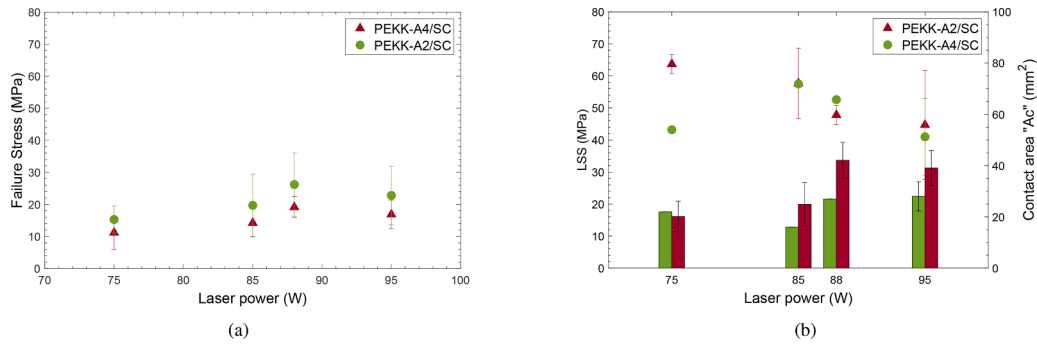


Fig. 12. Mechanical test results for each PEKK-A/SC assembly configuration: (a) failure stress for the SNJ failed assemblies, (b) lap shear stress (LSS) with their respective contact area (Ac) for the CI failed assemblies. Error bars indicate standard deviation.

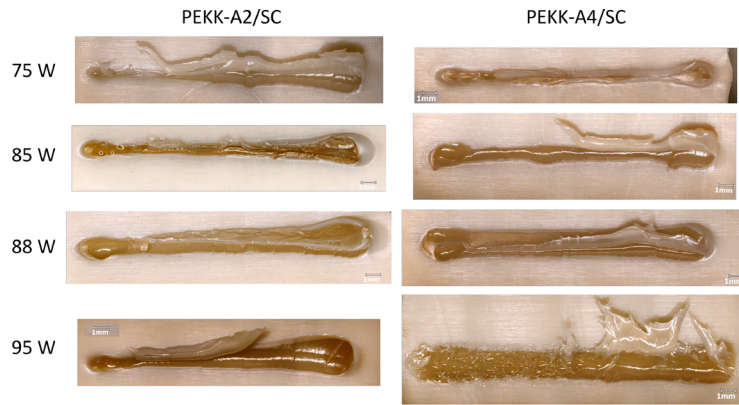


Fig. 13. Representative micrographs of the failed weld joint of assemblies failed with CI type for each assembly combination. Visualizations are made at the overlapped zone of the PEKK-SC sample.

The mean LSS of the CI failed assemblies is plotted with laser power in Fig. 12b with their respective  $A_c$ . The strength obtained for both types of assemblies (A2/SC and A4/SC) at one laser power is relatively the same, excepted for 75 W. However, contrary to the force at failure, LSS considerably decreases from 85 W. The maximum strength is reached at 85 W, with a value of 57 MPa, for both types of assemblies, whereas the minimum strength is obtained at 95 W, with  $43 \pm 2$  MPa. LSS decreases by 25 % between the maximum and minimum values for both types of assemblies. The explanation is that a high power intensity used for irradiation creates a bigger weld joint, obtaining a higher contact area. And, whereas the force at failure increases with power, the LSS will decrease because of the increment of contact area, this is noticeable in Fig. 12b. Overall, the strength obtained in the assemblies is higher than those achieved by Potente et al. when welding PEEK T-joint specimens with similar thicknesses for the transparent substrate Potente et al. (2001). They achieved a maximum strength of 40 MPa.

**Crystallized weld joints mechanical properties** Two powers are studied for the annealing process: 85 and 95 W, which are compared with the NC assemblies. Compared to the NC-PEKK assemblies, the annealed cold-crystallized (CC) ones, labeled as PEKK-Ac/SC, they all failed in SNJ type. In this case, the PEKK-A2c/SC failed within the PEKK-SC bulk sample, and the PEKK-A4c/SC failed at the initially (but now crystallized) PEKK-A4 amorphous bulk sample. Cohesive failure is not achieved when the crystallization is enhanced after welding. Nevertheless, the mechanical results can be studied and compared to the NC assemblies for the two laser powers mentioned and the two sample's thicknesses.

Fig. 14 compares the failure force with power for the NC and CC assemblies. The CC assemblies have a similar behavior as the NC ones: when the thickness of the PEKK-A increases, the resistance to the break load increases. Furthermore, the load at failure increases with crystallization whatever the power. For A2/SC assemblies, a 35 % increment is

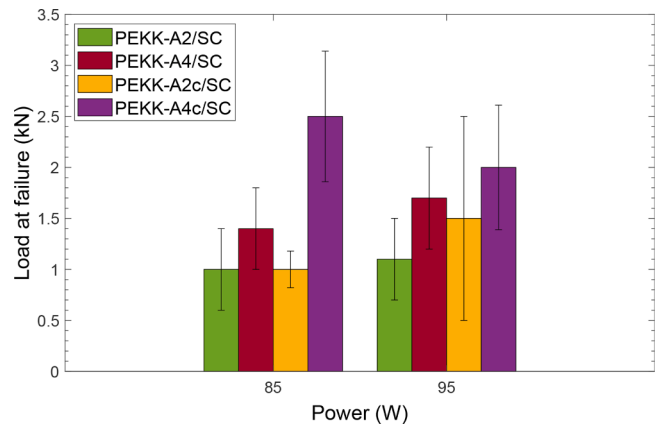
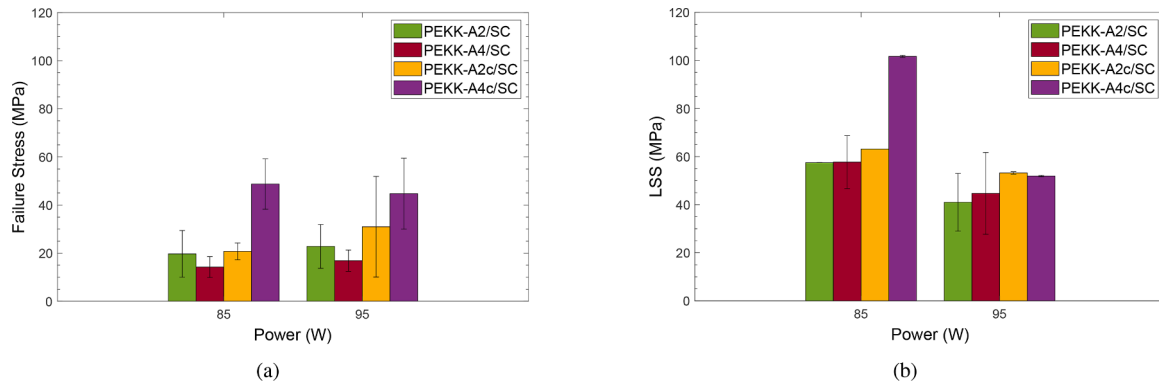


Fig. 14. Mechanical results of the PEKK annealed assemblies (PEKK-Ac/SC) showing the  $F_f$  compared with the correspondent PEKK non-annealed assemblies (PEKK-A/SC)  $F_f$ . Error bars indicate standard deviation.

observed between the non-crystallized and crystallized assemblies at 95W, while at 85W, the load at failure remains relatively the same. For the A4/SC assemblies, the breaking load increases by 19 % when welding with 95 W, and 81 % when using 85 W. This suggests a positive effect of annealing: the crystallized weld joints exhibit a higher resistance compared to the non-crystallized ones.

As previously, the failure stress can be calculated for the CC assemblies using the  $F_f$  and the  $A_f$ . Fig. 15a illustrates the failure stresses of both crystallized and non-crystallized assemblies. Similar to the trend observed for load at failure, the failure stress increases with the sample's thickness. Compared to the NC assemblies, the failure stress increases



**Fig. 15.** Mechanical tests results of the PEKK annealed assemblies (PEKK-Ac/SC) compared with the correspondent PEKK non-annealed assemblies (PEKK-A/SC) results: (a) failure stress and (b) lap shear stress. Error bars indicate standard deviation.

when enhancing crystallinity by annealing. However, contrary to the non-crystallized assemblies, it can be noticed that the failure stress is higher for the PEKK-A4c/SC than for the PEKK-A2c/SC. This change in the tensile resistance is due to the fact that, for CC assemblies, the load at break for the PEKK-A4c/SC is more than 70 % higher than for the PEKK-A2c/SC. Even though the PEKK-A4c/SC assemblies failed at the PEKK-A4 sample, the break load was high enough to achieve a high failure stress with a large failure area  $A_f = 48 \pm 3 \text{ mm}^2$ .

To obtain the weld strength of the CC assemblies, the force at failure is divided by the contact area of the weld. Because the welds are made in the same conditions as the initial non-crystallized (NC) ones, we assume the same contact area for all types of assembly. The average values of the PEKK-A/SC weld contact areas obtained for each laser assembly configuration were used to calculate the LSS for the crystallized assemblies. These LSS values are displayed in Fig. 15b and compared to the ones obtained for the PEKK-A/SC NC assemblies. The weld strength decreases with power for each assembly combination. Nevertheless, higher strength values are obtained for the crystallized assemblies. The strength of the assemblies increases by more than 10 % when fully crystallized. The higher increment is achieved for the PEKK-A4c/SC at 85 W, increasing by 76 % when crystallizing the weld joint, obtaining the maximum strength value at this power, reaching 102 MPa. The minimum laser power obtained is 52 MPa, being also higher than the minimum value obtained for the NC ones (41 MPa). To date, only one work in the literature reports the effect of annealing on LTW assemblies on similar material (PEEK) by Liu et al. (2022). In this work, the crystallized assemblies showed lower LSS values than the non-crystallized ones. More importantly, increasing the crystallinity of the weld joint had a negative impact on its strength. They obtained a maximum decrement of 7 % on the weld strength between the non-crystallized and the maximum crystallized weld joint. Their findings are opposite to the results obtained in the present work.

### Results of LTW modeling

Computational modeling is employed to gain insight into the intricate mechanisms of crystallization observed in the laser transmission welding experiments. The laser welding process is modeled for the PEKK-A2/SC-P1 assembly type, using the same parameters as the experimental tests, except for the power value. A perfect contact at the assembly interface is assumed to consider qualitatively the clamping pressure of the experiences. Only thermal simulations are done. The welding parameters set for the LTW modeling are indicated in Table 8.

The high-temperature gradient caused by laser power significantly alters the material's properties, making their exact values elusive. Studies have proven that thermal properties, such as the melting point of thermoplastic materials, decrease with high heating rates. Bölle et al. (2022) in 2022 demonstrated how the heating rate influences the

**Table 8**

Welding parameters for LTW modeling.

Parameter	Value
Laser power (P) [W]	15
Welding speed (V) [ $\text{mm s}^{-1}$ ]	1
Beam diameter (DB) [mm]	6
Weld length (Lw) [mm]	20
Cooling time (tc) [s]	120

melting peak position in PA66. The melting temperature of PA66 is modified at high heating rates, decreasing  $7^\circ\text{C}$  between a speed of 1 and  $100^\circ\text{C/s}$ . In addition, the simulations developed in the present study are based on a 1D absorption model perpendicular to the input surface with integration in Z, considering also the change in microstructure (crystallinity rate). The existing scattering in the parts is not incorporated in the model. A lower power value must be used then to reproduce, at best, the results obtained in the experimental tests for the PEKK-A2/SC-P1 assembly type in terms of weld joint morphology. This power value also corresponds to the power required to melt the volume of polymer within the weld seam, as calculated using the known thermal properties. In the preliminary tests of the simulations, 15 W was determined as the power value that allowed the welding tests to be explained in terms of weld joint morphology and crystallinity. This power value is also chosen based on a known model and parameters for semi-crystalline polymers.

Fig. 16 shows the temperature fields for two assembly views: the cross-section along the weld path and the assembly interface plan. The temperature is also shown for two different times of the simulated welding process: Fig. 16a corresponds to the first second of irradiation ( $t = 1 \text{ s}$ ), and Fig. 16b shows the last second of irradiation ( $t = 20 \text{ s}$ ). The cross-section along the weld path shows that the temperature field is non homogeneous between the upper and lower parts. At the beginning of irradiation ( $t = 1 \text{ s}$ ) (Fig. 16a), the highest temperatures are reached in the PEKK-SC bottom sample due to its high absorption properties compared to the PEKK-A upper part. It is also noticeable in the temperature distribution that the PEKK-SC part absorbed the energy in the volume, not only at the interface, as for the experimental tests. Then, this temperature field expands as the laser moves. As it can be seen at the end of the weld path (Fig. 16b), the PEKK-A sample now reaches high temperatures in its thickness and not only at the interface, but this thickness is still lower than that of the PEKK-SC sample. That indicates that both the PEKK-SC and PEKK-A melted in their volume at the irradiation process but within a different thickness, as observed experimentally with the ML of both parts. When visualizing the assembly interface plan, it can be noticed how the temperature evolution caused by the laser beam passes from a circular shape at the first second of irradiation to a comet shape at the end of the irradiation. The observed temperature distribution and its evolution along the welding process are

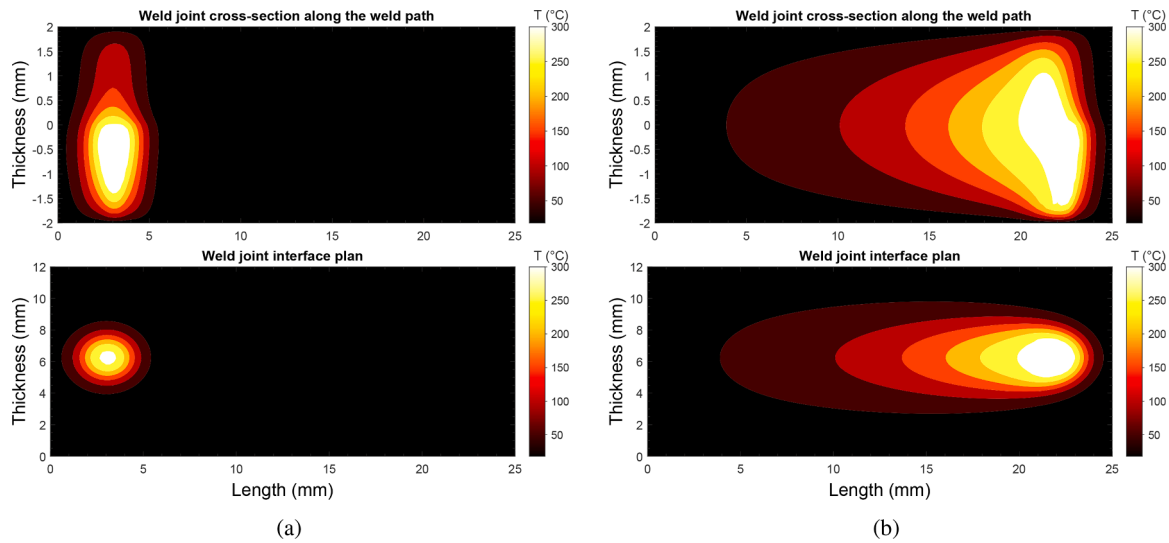


Fig. 16. Simulations results: Temperature field on the Weld joint at (a) 1s and (b) 20s of irradiation.

primarily attributed to the variation of the laser energy deposition at the assembly interface. The modification of the sample’s crystallinity caused by the increasing temperatures of the welding process makes the absorption coefficient evolve. This evolution in absorption capacities directly influence the energy deposition dynamics throughout the welding process.

Fig. 17 a shows two views of the weld joint HAZ after irradiation and cooling: the cross-section along the weld path and the interface plan. The isovalues indicate the crystallinity (Xc) of the samples. These numerical visualizations are comparable to those observed on the PEKK-A/SC NC assemblies. As observed experimentally in Fig. 6, two identifiable zones are also obtained in the simulations when visualizing the cross-section along the weld path (Fig. 17a top). An amorphous zone 1 covering both samples, and a cold crystallized zone 2 developed over zone 1. Then, when observing the HAZ at the interface plan for the CI failed assemblies in Fig. 13 it can be noticed that the weld joint is amorphous, as predicted by the numerical simulations at the bottom in Fig. 17a. Also, both experimental and numerical results indicate that the semi-crystalline polymer remains crystallized in the bottom zone. This behavior is attributed to the applied boundary conditions ( $T=18\text{ }^{\circ}\text{C}$ ) in the simulation. In the experiment, it is likely due to heat transfer with

the metallic support, which keeps this area near room temperature.

Fig. 17 b plots the temperature and crystallinity evolution in time for the two points indicated in the weld joint cross-section along the weld path of Fig. 17a: the center point of the assembly at the interface on the PEKK-SC part (wcp-int) with coordinates  $(x, y, z) = (12.5, 0, 0)$  mm, and the center point at the scL developed (wcp-scL) with coordinates  $(x, y, z) = (1.25, 0, 1.2)$  mm. At the interface, the temperature increases from ambient temperature ( $18\text{ }^{\circ}\text{C}$ ) to its maximum value (around  $314\text{ }^{\circ}\text{C}$ ) in less than 4 s, indicating a heating rate of  $100\text{ }^{\circ}\text{C/s}$ . The highest temperature reached is  $314\text{ }^{\circ}\text{C}$ , allowing melting of the material, as defined in the model, and as observed experimentally in section 2.4. Then, at the scL, the maximum temperature reached is about  $280\text{ }^{\circ}\text{C}$ , being lower than the melting temperature. That indicates that the PEKK-A sample did not melt in this zone. However, the elevated temperatures allowed the material to cold crystallize, agreeing with the experimental findings in section 2.4.

The variation of crystallinity (Xc) of the PEKK-SC (at the wcp-int) shows a drastic change from 24 % to almost zero when the melting temperature is reached. Then, with the temperature decrease, the crystallinity slightly increases up until it stabilizes at 9 %. That shows that the PEKK-SC sample melted upon irradiation and did not crystallize

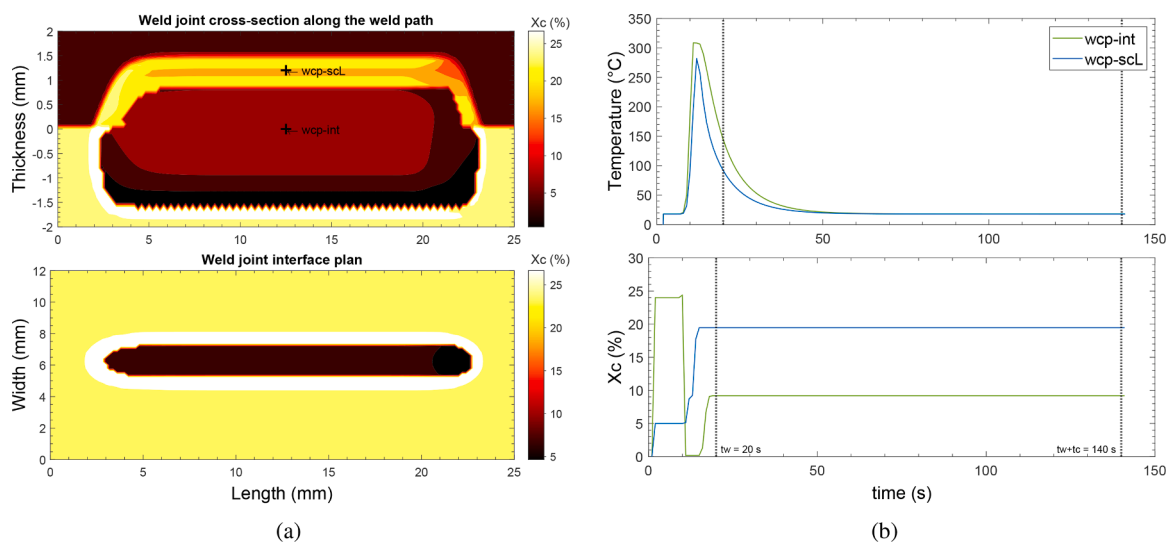


Fig. 17. Simulations results: (a) weld joint HAZ isovalues of the crystallinity after welding process, along the welding path and at the interface plans, and (b) plots of the temperature and the crystallinity degree over time.

during cooling, staying amorphous. On the other side, at the PEKK-A sample (the wcp-sCL point), the crystallinity increases with temperature, reaching a maximum of 20 %. This indicates that the PEKK-A part achieved cold crystallization during irradiation, achieving a semi-crystalline state as stated in the sCL. These numerical results are in accordance and comparable with the experimental results obtained.

## Conclusion

This study provides a comprehensive analysis of LTW of PEKK assemblies, in an amorphous over semi-crystalline configuration (PEKK-A/SC). Through experimental characterization and numerical modeling, the relationships between material crystallinity, process parameters and weld joint properties are assessed. The process parameters influence the joint morphology and mechanical resistance of welds. The effect of crystallinity on the weld joint strength is clarified by conducting post-weld annealing in some welds. The following conclusions can be outlined from the results:

- The weld joint shows an anisotropic distribution of the crystallinity within its HAZ. Two different zones are identified in the weld joint HAZ that are correlated with the thermal history of the welding process: an amorphous zone 1, also named “molten layer” (ML); and the cold-crystallized zone 2, named “semi-crystalline layer” (sCL).
- The depth and morphology of the molten and semi-crystalline layers show significant variations depending on laser power and semi-transparent part thickness.
- Mechanical testing revealed two failure types: cohesive (CI) and substrate near joint (SNJ), which reveal the weld properties, as well as the failure mechanisms.
- The mechanical strength of the PEKK-A/SC weld joints decreases with laser power. High values are reached between 41 and 64 MPa.
- Crystallization of the welds is achieved by annealing without joint separation. This crystallization generates an homogeneous crystallized HAZ with different crystalline structure, due to cold crystallization of the ML.
- Enhancing the crystallinity of welds by annealing improves their mechanical strength, demonstrating the potential of post-weld treatments to optimize weld performance. Higher values of LSS are thus obtained, between 52 and 102 MPa.
- Modelling the LTW process by finite difference method allows for a better understanding of this complex mechanism of crystallization observed during welding experiments. We demonstrate the possibility to predict the weld joint morphology depending on material properties and process parameters.
- Overall, controlling the crystallization properties and kinetics of PEKK is crucial to achieve optimal welding and to predict the weld joint properties.

This research provides a deep understanding of the fundamental mechanisms governing the formation and properties of weld joints in LTW PEKK assemblies. The outcomes contribute to boost the development of LTW for assembling high-performance semi-crystalline thermoplastic for various applications across high demanding industrial sectors.

## Declaration of generative AI and AI-assisted technologies in the writing process

During the preparation of this work the author(s) used ChatGPT 3.5 in order to improve writing language and clarity. After using this tool/service, the author(s) reviewed and edited the content as needed and take(s) full responsibility for the content of the publication.

## CRedit authorship contribution statement

**Marcela Matus-Aguirre:** Conceptualization, Investigation, Methodology, Formal analysis, Data curation, Visualization, Software, Writing – original draft. **Benôit Cosson:** Conceptualization, Methodology, Software, Supervision, Validation, Writing – review & editing. **Christian Garnier:** Conceptualization, Methodology, Validation, Writing – review & editing. **Fabrice Schmidt:** Conceptualization, Validation, Writing – review & editing. **André Chateau Akué-Asséko:** Conceptualization, Validation, Writing – review & editing. **France Chabert:** Conceptualization, Supervision, Validation, Writing – review & editing, Funding acquisition.

## Declaration of competing interest

The authors declare that they have no known competing financial interests or personal relationships that could have appeared to influence the work reported in this paper.

## Data availability

Data will be made available on request.

## Acknowledgments

The PhD fellowship was attributed to Marcela Matus Aguirre by the Occitanie region of France through the PLASC project and by IMT Nord Europe. The authors are grateful to Rémi Gilblas, research engineer at IMT Mines Albi, for helping with the optical characterization of the PEKK plates; to Damien Thierry, intern at ENIT, for helping with the characterization of the PEKK crystallized assemblies; and to Guillaume Morel, technician at ENIT, for helping with injection molding of PEKK plates. The authors sincerely thank Arkema company for supplying PEKK pellets and for the fruitful discussion.

## References

- Abed, S., Laurens, P., Carrétéro, C., Deschamps, J.R., Duval, C., 2001. Diode laser welding of polymers: microstructures of the welded zones for polypropylene. International Congress on Applications of Lasers & Electro-Optics. Laser Institute of America, Jacksonville, Florida, USA, pp. 1499–1507. <https://doi.org/10.2351/1.5059820>.
- Acherjee, B., 2020. Laser transmission welding of polymers—A review on process fundamentals, material attributes, weldability, and welding techniques. *J. Manuf. Processes* 60, 227–246.
- Acherjee, B., Kuar, A.S., Mitra, S., Misra, D., 2011. Modeling and analysis of simultaneous laser transmission welding of polycarbonates using an fem and rsm combined approach. *Opt. Laser Technol.* 44 (4), 995–1006.
- Acherjee, B., Kuar, A.S., Mitra, S., Misra, D., 2012. Modeling of laser transmission contour welding process using fea and doe. *Opt. Laser Technol.* 44 (5), 1281–1289.
- Ahmed, H., van Tooren, M., Justice, J., Harik, R.F., Kidane, A., Reynolds, A., 2018. Investigation and development of friction stir welding process for unreinforced polyphenylene sulfide and reinforced polyetheretherketone. *J. Thermoplast. Compos. Mater.* 32, 1242–1267. <https://api.semanticscholar.org/CorpusID:53652291>
- Amanat, N., Chaminade, C., Grace, J., James, N.L., McKenzie, D.R., 2011. Optimal process parameters for thermoplastic polyetheretherketone joints fabricated using transmission laser welding and Lumogen® IR absorptive pigment. *J. Laser Appl.* 23 (1), 012003 <https://doi.org/10.2351/1.3552972>. Publisher: Laser Institute of America. <https://lia.scitation.org/doi/full/10.2351/1.3552972>
- Amanat, N., Chaminade, C., Grace, J., McKenzie, D.R., James, N.L., 2010. Transmission laser welding of amorphous and semi-crystalline poly-ether-ether-ketone for applications in the medical device industry. *Mater. Des.* 31 (10), 4823–4830. <https://doi.org/10.1016/j.matdes.2010.04.051>. <https://linkinghub.elsevier.com/retrieve/pii/S0261306910002621>
- Arkema France. KEPSTAN technical data - KEPSTAN 7000 series. Arkema France. 2021.
- Bachmann, F.G., Russek, U.A., 2002. Laser welding of polymers using high-power diode lasers. Photon processing in Microelectronics and Photonics, 4637. SPIE, pp. 505–518.
- Blundell, D.J., Osborn, B.N., 1983. The morphology of poly(aryl-ether-ether-ketone). *Polymer* 24 (8), 953–958. [https://doi.org/10.1016/0032-3861\(83\)90144-1](https://doi.org/10.1016/0032-3861(83)90144-1). <https://www.sciencedirect.com/science/article/pii/0032386183901441>

- Bölle, S., Alms, J., Weihermüller, M., Robisch, M., Wipperfurth, J., Hopmann, C., Dahlmann, R., 2022. Modelling of the melting point shift in semi-crystalline thermoplastics dependent on prior cooling rate and heating rate. *Polymer* 254, 125100.
- Broek, C., 2015. Optimising ultrasonic welding of carbon fibre PEKK composites. Carassus, F., Korycki, A., Garnier, C., Chabert, F., Yahiaoui, M., Djilali, T., 2023. Influence of roughness in ultrasonic welding of carbon fiber/PEEK composites. *Mater. Res. Proc.* 28, 1841–1850. <https://doi.org/10.21741/9781644902479-199>.
- Chabert, F., Garnier, C., Sangleboeuf, J., Akue Asseko, A.C., Cosson, B., 2020. Transmission laser welding of polyamides: effect of process parameter and material properties on the weld strength. *Procedia Manuf.* 47, 962–968. <https://doi.org/10.1016/j.promfg.2020.04.297>. 23rd International Conference on Material Forming
- Cheng, S.Z.D., Ho, R., Hsiao, B.S., Gardner, K.H., 1996. Polymorphism and crystal structure identification in poly(aryl ether ketone ketone)s. *Macromol. Chem. Phys.* 197, 185–213. <https://api.semanticscholar.org/CorpusID:96965090>
- Choupin, T., Payolle, B., Régner, G., Paris, C., Cinquin, J., Brulé, B., 2018. A more reliable DSC-based methodology to study crystallization kinetics: application to poly(ether ketone ketone) (PEKK) copolymers. *Polymer* 155, 109–115. <https://doi.org/10.1016/j.polymer.2018.08.060>. <https://www.sciencedirect.com/science/article/pii/S0032386118308061>
- Coelho, J.M.P., Abreu, M., Rodrigues, F.C., 2003. Thermal modeling CO<sub>2</sub> laser radiation transmission welding of superposed thermoplastic films. *Opt. Eng.* 42, 3365–3373. <https://api.semanticscholar.org/CorpusID:121768923>
- Coelho, J.M.P., Abreu, M., Rodrigues, F.C., 2004. Methodologies for determining thermoplastic films optical parameters at 10.6 μm laser wavelength. *Polym. Test.* 23, 307–312. <https://api.semanticscholar.org/CorpusID:136624623>
- Cosson, B., Schmidt, F., Maoult, Y.L., 2009. Numerical infrared heating of semi transparent thermoplastic using ray tracing method. *Int. J. Mater. Form.* 2, 267–270. <https://api.semanticscholar.org/CorpusID:135824032>
- Doumeng, M., Makhlof, L., Berthet, F., Marsan, O., Delbé, K., Denape, J., Chabert, F., 2021. A comparative study of the crystallinity of polyetheretherketone by using density, dsc, xrd, and raman spectroscopy techniques. *Polym. Test.* 93, 106878.
- Dubé, M., Chazerain, A., Hubert, P., Yousefpour, A., Bersee, H.E., 2015. Characterization of resistance-welded thermoplastic composite double-lap joints under static and fatigue loading. *J. Thermoplast. Compos. Mater.* 28 (6), 762–776.
- Dubé, M., Hubert, P., Gallet, J.N., Stavrov, D., Bersee, H.E., Yousefpour, A., 2008. Fatigue performance characterisation of resistance-welded thermoplastic composites. *Compos. Sci. Technol.* 68 (7–8), 1759–1765.
- Dubé, M., Hubert, P., Gallet, J.N., Stavrov, D., Bersee, H.E., Yousefpour, A., 2012. Metal mesh heating element size effect in resistance welding of thermoplastic composites. *J. Compos. Mater.* 46 (8), 911–919.
- Flanagan, M., Doyle, A., Doyle, K., Ward, M., Bizeul, M., Canavan, R., Weafer, B., Brádaigh, C.M.Ó., Harrison, N.M., Goggins, J., 2018. Comparative manufacture and testing of induction-welded and adhesively bonded carbon fibre PEKK stiffened panels. *J. Thermoplast. Compos. Mater.* 32, 1622–1649. <https://api.semanticscholar.org/CorpusID:139488146>
- France, A., 2024. Pekk polyetherketoneketone. Accessed on March 08th, 2024. <https://www.arkema.com/global/en/products/product-families/pekk-kepstan/>
- Gardner, K.H., Hsiao, B.S., Faron, K.L., 1994. Polymorphism in poly(aryl ether ketone) s. *Polymer* 35 (11), 2290–2295.
- Gardner, K.H., Hsiao, B.S., Matheson, R.R., Wood, B.A., 1992. Structure, crystallization and morphology of poly(aryl ether ketone ketone). *Polymer* 33 (12), 2483–2495.
- Ghorbel, E., Casalino, G., Abed, S., 2009. Laser diode transmission welding of polypropylene: geometrical and microstructure characterisation of weld. *Mater. Des.* 30 (7), 2745–2751.
- Gonçalves, L.F., Duarte, F.M., Martins, C.I., Paiva, M.C., 2021. Laser welding of thermoplastics: an overview on lasers, materials, processes and quality. *Infrared Phys. Technol.* 119, 103931.
- González, I., Sanz, A., Fernandez, A.R., 2014. Characterization of metal heating elements for resistance welding of thermoplastic matrix composites (PEEK). *Mater. Sci. Forum* 797, 104–199. <https://api.semanticscholar.org/CorpusID:136975614>
- Goyal, D.K., Kant, R., 2023. Mechanism of bonding during laser transmission welding using EIP absorber. *Mater. Manuf. Processes* 38 (4), 485–493. <https://doi.org/10.1080/10426914.2023.2165676>. <https://www.tandfonline.com/doi/full/10.1080/10426914.2023.2165676>
- Grouve, W., Vrugink, E., Sacchetti, F., Akkerman, R., 2020. Induction heating of UD C/PEKK cross-ply laminates. *Procedia Manuf.* 47, 29–35.
- Ho, R., Cheng, S.Z.D., Hsiao, B.S., Gardner, K.H., 1995. Crystal morphology and phase identification in poly(aryl ether ketone)s and their copolymers. 3. Polymorphism in a polymer containing alternated terephthalic acid and isophthalic acid isomers. *Macromolecules* 28, 1938–1945. <https://api.semanticscholar.org/CorpusID:98317121>
- Ho, R.-M., Cheng, S.Z., Hsiao, B.S., Gardner, K.H., 1994. Crystal morphology and phase identifications in poly(aryl ether ketone) s and their copolymers. 1. Polymorphism in PEKK. *Macromolecules* 27 (8), 2136–2140.
- Hsiao, B.S., Gardner, K.H., Cheng, S.Z., 1994. Crystallization of poly(aryl ether ketone ketone) copolymers containing terephthalate/isophthalate moieties. *J. Polym. Sci. Part B* 32 (16), 2585–2594.
- Jeong, J., Lee, D., Ju, H., Kweon, J., Nam, Y., 2023. Effect of hygrothermal condition on single-lap shear behavior of induction-welded CF/PEKK thermoplastic composites. *Adv. Compos. Mater.* 32 (5), 657–673.
- Jones, I.A., 2002. Laser welding for plastic components. *Assembly Autom.* 22, 129–135. <https://api.semanticscholar.org/CorpusID:110538490>
- Jose, J.V., Panneerselvam, K., 2021. Joining of PEEK plates by friction stir welding process. *Mater. Today: Proceedings* 39 (4), 1635–1639. <https://doi.org/10.1016/j.matpr.2020.05.768>
- Kagan, V., Bray, R.G., 2001. Advantages and limitations of laser welding technology for semi-crystalline reinforced plastics. International Congress on Applications of Lasers & Electro-Optics. Laser Institute of America, Jacksonville, Florida, USA, pp. 1218–1227. <https://doi.org/10.2351/1.5059784>. <http://aip.scitation.org/doi/abs/10.2351/1.5059784>
- Kagan, V.A., Bray, R.G., Kuhn, W.P., 2002. Laser transmission welding of semi-crystalline thermoplastics—Part I: optical characterization of nylon based plastics. *J. Reinf. Plast. Compos.* 21 (12), 1101–1122. <https://doi.org/10.1177/073168402128987699>. <http://journals.sagepub.com/doi/10.1177/073168402128987699>
- Köhler, F., Villegas, I.F., Dransfeld, C., Herrmann, A., 2021. Static ultrasonic welding of carbon fibre unidirectional thermoplastic materials and the influence of heat generation and heat transfer. *J. Compos. Mater.* 55 (15), 2087–2102.
- Korycki, A., Carassus, F., Garnier, C., Chabert, F., Djilali, T., 2023. Effect of energy director thickness on thermal diffusion and joint quality during ultrasonic welding of CF/PEEK composites. *Mater. Res. Proc.* 28, 1819–1828. <https://doi.org/10.21741/9781644902479-197>
- Korycki, A., Garnier, C., Bonmatin, M., Laurent, E., Chabert, F., 2022. Assembling of carbon fibre/PEEK composites: comparison of ultrasonic, induction, and transmission laser welding. *Materials* 15 (18), 6365. <https://doi.org/10.3390/ma15186365>. Number: 18 Publisher: Multidisciplinary Digital Publishing Institute
- Kosloh, J., Sackmann, J., Schomburg, W.K., 2017. Ultrasonic fabrication of micro fluidic channels from polyether ether ketone (PEEK). *Microsyst. Technol.* 23, 5505–5513. <https://api.semanticscholar.org/CorpusID:136184054>
- Kwon, B., Choe, H., Jeong, J., Ju, H., Kweon, J.-H., Nam, Y.-W., 2021. Static and fatigue behavior of induction-welded single lap carbon fiber reinforced polyetherketoneketone thermoplastic composite joints. *J. Compos. Mater.* 55 (28), 4183–4193.
- Liu, Y., Zhang, W., Liu, J., Guan, Y., Ding, X., 2022. Study on microstructures and mechanical performance of laser transmission welding of poly-ether-ether-ketone (PEEK) and carbon fiber reinforced PEEK (CFR-PEEK). *J. Laser Appl.* 34 (4), 042037. <https://doi.org/10.2351/7.0000823>
- Ma, W., Zhan, X., Yang, H., Bu, H., Li, Y.C., Wang, F., 2020. Study on the interface morphology in the induction welding joint of PEEK plate at low power. *J. Polym. Eng.* 40, 432–439. <https://api.semanticscholar.org/CorpusID:218668146>
- Mamuschkin, V., Olowinsky, A., Britten, S.W., Engelmann, C., 2014. Investigations on laser transmission welding of absorber-free thermoplastics. Laser-based Micro-and Nanoprocessing VIII, 8968. SPIE, pp. 224–232.
- Matus Aguirre, M., 2023. Laser transmission welding of PEKK: influence of material properties and process parameters on the weld strength. pp. 1829–1840. <https://www.mrforum.com/product/9781644902479-198>. 10.21741/9781644902479-198.
- Modi, V., Bandaru, A.K., Ramaswamy, K., Kelly, C., McCarthy, C., Flanagan, T., O'Higgins, R., 2023. Repair of impacted thermoplastic composite laminates using induction welding. *Polymers* 15 (15), 3238.
- Mongan, P.G., Modi, V., McLaughlin, J.W., Hinchey, E.P., O'Higgins, R.M., O'Dowd, N.P., McCarthy, C.T., 2022. Multi-objective optimisation of ultrasonically welded dissimilar joints through machine learning. *J. Intell. Manuf.* 33 (4), 1125–1138.
- Pereira, A.B., Fernandes, F.A.O., de Moraes, A.B., 2019. Mechanical Strength of Thermoplastic Polyamide Welded by Nd:YAG Laser. *Polymers* 11 (9), 1381. <https://doi.org/10.3390/polym11091381>
- Perez-Martin, H., Mackenzie, P., Baidak, A., Brádaigh, C.M.Ó., Ray, D., 2021. Crystallinity studies of PEKK and carbon fibre/PEKK composites: a review. *Compos. Part B* 223, 109127.
- Potente, H., Becker, F., Fiegler, G., Korte, J., 2001. Investigations towards application of a new technique on laser transmission welding. *Weld. World* 45 (5–6), 15–20.
- Pérez-Martin, H., Mackenzie, P., Baidak, A., Brádaigh, C.M., Ray, D., 2022. Crystallisation behaviour and morphological studies of PEKK and carbon fibre/PEKK composites. *Compos. Part A* 159, 106992. <https://doi.org/10.1016/j.compositesa.2022.106992>. <https://linkinghub.elsevier.com/retrieve/pii/S1359835X22001804>
- Quiroga Cortés, L., Caussé, N., Dantras, E., Lonjon, A., Lacabanne, C., 2016. Morphology and dynamical mechanical properties of poly ether ketone ketone (PEKK) with meta phenyl links. *J. Appl. Polym. Sci.* 133, 43396. <https://doi.org/10.1002/app.43396>
- Russello, M., Catalanotti, G., Hawkins, S., Falzon, B.G., 2023. Resistance welding of carbon fibre reinforced PEKK by means of CNT webs. *J. Compos. Mater.* 57 (1), 79–94.
- Shi, H., Villegas, I.F., Bersee, H., 2013. Strength and failure modes in resistance welded thermoplastic composite joints: effect of fibre-matrix adhesion and fibre orientation. *Compos. Part A* 55, 1–10.
- Villar, M., Garnier, C., Chabert, F., Nassiet, V., Samélor, D., Diez, J.C., Sotelo, A., Madre, M.A., 2018. In-situ infrared thermography measurements to master transmission laser welding process parameters of PEKK. *Opt. Lasers Eng.* 106, 94–104. <https://doi.org/10.1016/j.optlaseng.2018.02.016>. <https://www.sciencedirect.com/science/article/pii/S0143816617308977>
- Xu, X.F., Bates, P.J., Zak, G., 2015. Effect of glass fiber and crystallinity on light transmission during laser transmission welding of thermoplastics. *Opt. Laser Technol.* 69, 133–139. <https://api.semanticscholar.org/CorpusID:121616193>
- Xu, X.F., Parkinson, A., Bates, P.J., Zak, G., 2015. Effect of part thickness, glass fiber and crystallinity on light scattering during laser transmission welding of thermoplastics. *Opt. Laser Technol.* 75, 123–131. <https://doi.org/10.1016/j.optlaseng.2015.06.026>. <https://www.sciencedirect.com/science/article/pii/S0030399215001887>